



pubs.acs.org/cm Perspective

# A "Tips and Tricks" Practical Guide to the Synthesis of Metal Halide Perovskite Nanocrystals

Yangning Zhang, Timothy D. Siegler, Cherrelle J. Thomas, Michael K. Abney, Tushti Shah, Anastacia De Gorostiza, Randalynn M. Greene, and Brian A. Korgel\*



Cite This: Chem. Mater. 2020, 32, 5410-5423



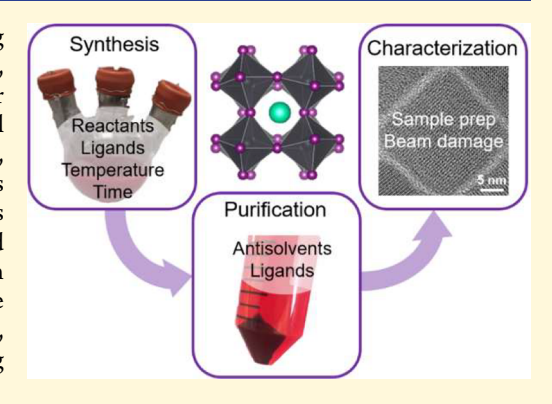
**ACCESS** 

III Metrics & More

Article Recommendations

sı Supporting Information

ABSTRACT: Metal halide perovskite nanocrystals offer a range of interesting properties and are being studied extensively for applications in solar cells, photodetectors and light-emitting devices. This perspective provides a number of best practices for the synthesis, purification, and characterization of metal halide perovskite nanocrystals, with detailed discussion of CsPbI<sub>3</sub>, CsPbBr<sub>3</sub>, CH<sub>3</sub>NH<sub>3</sub>PbI<sub>3</sub> (MAPI), and Cs<sub>2</sub>AgBiBr<sub>6</sub> as examples. The choice of reactants and ligands for hot-injection reactions are discussed, as well as how various reaction conditions, including temperature and time, affect yield, uniformity, and crystal phase. We extensively discuss the use of antisolvent precipitation methods for purification, since ligand coordination to most perovskite nanocrystals is weak and the nanocrystals are sensitive to degradation. Finally, we discuss some of the strategies for imaging these nanocrystals using transmission electron microscopy (TEM).



## ■ INTRODUCTION

Metal halide (ABX<sub>3</sub>) perovskites are composed of monovalent A<sup>+</sup> cations, such as Cs<sup>+</sup>, CH<sub>3</sub>NH<sub>3</sub><sup>+</sup>, or CH(NH<sub>2</sub>)<sub>2</sub><sup>+</sup>, bivalent B<sup>2+</sup> Group IVA metal cations, such as Pb<sup>2+</sup>, Sn<sup>2+</sup>, or Ge<sup>2+</sup>, and halide X<sup>-</sup> anions, such as Cl<sup>-</sup>, Br<sup>-</sup>, or I<sup>-</sup>, positioned in a three-dimensional network of linked, corner-sharing [BX<sub>6</sub>]<sup>4-</sup> octahedra with A<sup>+</sup> cations in the interstices. Ligand-stabilized nanocrystals of CsPbX<sub>3</sub>, A<sup>3,4</sup> Cs<sub>x</sub>Rb<sub>1-x</sub>PbX<sub>3</sub>, and lead-free double perovskites Cs<sub>2</sub>AgBiBr<sub>6</sub>, Cs<sub>2</sub>AgSbCl<sub>6</sub>, Cs<sub>2</sub>AgInCl<sub>6</sub>, and Cs<sub>2</sub>NaInCl<sub>6</sub> have been made, as well as organic-inorganic hybrids of CH<sub>3</sub>NH<sub>3</sub>PbX<sub>3</sub> (i.e., MAPbX<sub>3</sub>), All CH(NH<sub>2</sub>)<sub>2</sub>PbX<sub>3</sub> (i.e., FAPbX<sub>3</sub>), All and (RNH<sub>3</sub>)<sub>2</sub>(MA)<sub>n-1</sub>Pb<sub>n</sub>X<sub>3n+1</sub>. These have exhibited high photoluminescence quantum yield (PL QY), All Shift bright exciton triplet states, superfluorescence, as well as promising performance in photovoltaics (PVs), Close as well as promising performance in photovoltaics (PVs), All Shift bright excitons and rapidly emerging research area.

One challenge with doing research on an up-and-coming class of nanomaterials is that the best practices for synthesis seem to evolve with each additional publication. We have found that strictly following many published protocols—especially from older papers—often results in perovskite nanocrystals that rapidly degrade within a few hours or have the wrong crystal structure or low PL QYs. Key information and fresh insights are constantly evolving.

This perspective highlights a number of "tips and tricks" that we have learned regarding the synthesis, purification, and characterization of metal halide perovskite nanocrystals and hopefully will provide helpful guidance, especially for researchers relatively new to the field. The discussion focuses on four specific types of nanocrystals: CsPbI<sub>3</sub>, CsPbBr<sub>3</sub>, MAPbI<sub>3</sub>, and Cs<sub>2</sub>AgBiBr<sub>6</sub>. These materials exhibit many similar characteristics in terms of their synthesis and handling yet also provide their own unique challenges, thus, providing an illustration of some of the fundamental aspects of metal halide perovskite nanocrystal synthesis.

### SYNTHETIC PATHWAYS

Figure 1 lists various reactions involved in the synthesis of CsPbI<sub>3</sub>, CsPbBr<sub>3</sub>, MAPbI<sub>3</sub>, and Cs<sub>2</sub>AgBiBr<sub>6</sub> nanocrystals. We start this perspective with a discussion of CsPbI<sub>3</sub>, as it provides one of the most interesting examples of perovskite stability in nanocrystals.

**CsPbI<sub>3</sub> Nanocrystals.** The equilibrium phase of CsPbI<sub>3</sub> at room temperature is not a perovskite—it is an optically inactive,  $\delta$ -orthorhombic phase with a yellow color. The equilibrium phase of CsPbBr<sub>3</sub> is a perovskite, which makes it much more stable and easier to synthesize than CsPbI<sub>3</sub> nanocrystals. Option 1 is actually remarkable that perovskite

Received: April 23, 2020 Revised: June 15, 2020 Published: June 16, 2020





#### A. Oleate injection method

#### 1. Formation of metal-oleate:

$$Cs_2CO_3 + 2RCOOH \longrightarrow 2Cs(RCOO) + CO_2 + H_2O$$
 (1)

# 2. Formation of perovskite and by-product:

$$2 Cs(RCOO) + 3PbI_2 \longrightarrow 2 CsPbI_3 + Pb(RCOO)_2 \qquad (2)$$

$$PbX_2 + 2RCOOH + 2R'NH_2 \longrightarrow Pb(OOCR)_2 + 2R'NH_3X \quad (X=Br, I) \qquad (2a)$$

$$Cs(RCOO) + Pb(RCOO)_2 + 3R'NH_3X \longrightarrow CsPbX_3 + 3R'NH_3OOCR \quad (X=Br, I) \qquad (2b)$$

$$2 Cs(RCOO) + 3PbBr_2 \longrightarrow 2 CsPbBr_3 + Pb(RCOO)_2 \qquad (3)$$

$$2 CH_3NH_2 + 2RCOOH + 3PbI_2 \longrightarrow 2 CH_3NH_3PbI_3 + Pb(RCOO)_2 \qquad (4)$$

$$3AgBr + 3BiBr_3 + 4Cs(RCOO) \longrightarrow 2 Cs_3AgBiBr_6 + Ag(RCOO) + Bi(RCOO)_3 \qquad (5)$$

#### B. TMS-X injection method

# 1. Formation of metal-oleate:

$$C_{82}CO_3 + 2RCOOH \longrightarrow 2C_8(RCOO) + CO_2 + H_2O \qquad (6)$$

$$PbO + 2RCOOH \longrightarrow Pb(RCOO)_2 + H_2O \qquad (7)$$

$$AgOOCCH_3 + RCOOH \longrightarrow Ag(RCOO) + CH_3COOH \qquad (8)$$

$$Bi(OOCCH_3)_3 + 3RCOOH \longrightarrow Bi(RCOO)_3 + 3CH_3COOH \qquad (9)$$

## 2. Formation of OAm-X (X=Br, I):

$$(CH_3)_3SiX + RCOOH \longrightarrow RCOOSi(CH_3)_3 + HX$$
 (10)  
 $(CH_3)_3SiX + R'NH_2 \longrightarrow R'NHSi(CH_3)_3 + HX$  (11)  
 $HX + R'NH_2 \longrightarrow R'NH_3X$  (12)

# 3. Formation of perovskite and by-product:

$$Cs(RCOO) + Pb(RCOO)_2 + 3R'NH_3I \longrightarrow CsPbI_3 + 3R'NH_3OOCR \qquad (13)$$

$$Cs(RCOO) + Pb(RCOO)_2 + 3R'NH_3Br \longrightarrow CsPbBr_3 + 3R'NH_3OOCR \qquad (14)$$

$$CH_3NH_2 + RCOOH + Pb(RCOO)_2 + 3R'NH_3I \longrightarrow CH_3NH_3PbI_3 + 3R'NH_3OOCR \qquad (15)$$

$$2Cs(RCOO) + Ag(RCOO) + Bi(RCOO)_3 + 6R'NH_3Br \longrightarrow Cs_2AgBiBr_6 + 6R'NH_3OOCR \qquad (16)$$

$$2Cs(RCOO) + Ag(RCOO) + Bi(RCOO)_3 + 6 (CH_3)_3SiBr \longrightarrow Cs_2AgBiBr_6 + 6 (CH_3)_3SiOOCR \qquad (17)$$

$$R = CH_3(CH_2)_7HC = CH(CH_2)_7 \qquad R' = CH_3(CH_3)_7HC = CH(CH_2)_8$$

Figure 1. Reactions involved in the synthesis of CsPbBr<sub>3</sub>, CsPbI<sub>3</sub>, CH<sub>3</sub>NH<sub>3</sub>PbI<sub>3</sub> (MAPI), and Cs<sub>2</sub>AgBiBr<sub>6</sub> nanocrystals by hot injection of metaloleate, methylamine, or trimethylsilyl halide (TMS-X).

CsPbI<sub>3</sub> nanocrystals can be obtained by colloidal synthesis, since they are inhabiting a metastable phase.<sup>3,20,21</sup>

CsPbI<sub>3</sub> nanocrystals are commonly prepared by ionic metathesis, as shown in eq 2 in Figure 1, in oleic acid (OA), oleylamine (OAm), and octadecene (ODE) by hot injection. One pot or heat-up methods are rarely used because metal halide perovskite nanocrystals have fast reaction and nucleation kinetics, and the reaction time cannot be controlled sufficiently to prevent broadening of the size and shape distribution, aggregation, or formation of undesired phases, such as the yellow  $\delta$ -orthorhombic phase. ODE serves as a high boiling inert solvent; OAm is the primary capping ligand; and OA participates in the metathesis reaction, although it can also adsorb to the nanocrystal surface as a capping ligand.

A typical synthesis involves the dissolution of  $PbI_2$  in OA, OAm, and ODE at 120 °C, before setting the reaction temperature somewhere between 120 and 180 °C. As shown in eq 2a in Figure 1, this step generates Pb-oleate and oleylammonium iodide (OAm-I). Cs-oleate reactant is

prepared separately by combining Cs<sub>2</sub>CO<sub>3</sub> with oleic acid (eq 1, Figure 1). Cs-oleate in ODE is then heated and injected into the mixture of Pb-oleate and OAm-I to trigger the formation of CsPbI<sub>3</sub> and oleylammonium oleate (eq 2b, Figure 1). As shown in eq 2 in Figure 1, CsPbI<sub>3</sub> nanocrystals are produced with Pb-oleate as a byproduct.<sup>3,21</sup> A stoichiometric excess of PbI<sub>2</sub> relative to CsPbI<sub>3</sub> is required to drive the metathesis reaction to completion. A typical reaction using 20 mL of ODE yields about 130 mg of CsPbI<sub>3</sub> nanocrystals, corresponding to 30% molar conversion of reactants. Reactions can also be performed by injecting PbI<sub>2</sub> complexed with trioctylphosphine (TOP) into ODE solutions of OA, OAm, and Cs-oleate at 100–170 °C.<sup>42</sup> The major drawback of this method is that it takes a long time—about a week—to form the TOP-PbI<sub>2</sub> complex.

 $CsPbI_3$  nanocrystals can also be made by decoupling the  $Pb^{2+}$  and  $I^-$  sources and starting with PbO and an  $I^-$  precursor, such as trimethylsilyl iodide (TMSI), benzoyl iodide, OAm-I, or  $GeI_2.^{43-46}$  Cs-oleate and Pb-oleate are prepared separately

by dissolving Cs<sub>2</sub>CO<sub>3</sub> and PbO in OA (eqs 6 and 7, Figure 1) and then adding the solution to OAm and ODE. CsPbI<sub>3</sub> nucleation and growth is triggered by injecting TMSI into the reaction mixture at 150 °C. TMSI reacts with oleic acid and oleylamine to release HI, TMS-oleate, and TMS-oleylamine byproducts. HI further reacts with oleylamine to form OAm-I (eqs 10–12, Figure 1), which ultimately reacts with Cs-oleate and Pb-oleate to produce CsPbI<sub>3</sub> nanocrystals and oleylammonium oleate as a byproduct (eq 13, Figure 1). This reaction in 5 mL of ODE makes about 25 mg of nanocrystals (37% yield).

Figure 2a,b shows TEM images of CsPbI<sub>3</sub> nanocrystals synthesized by Cs-oleate or TMSI injection. UV-vis

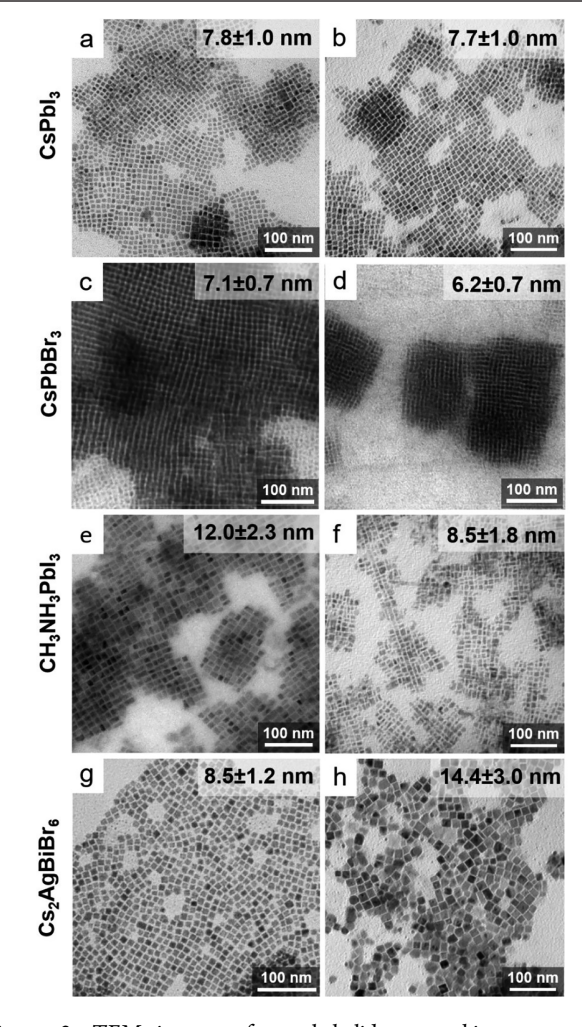


**Figure 2.** TEM images of metal halide perovskite nanocrystals synthesized by injection of (a, c, e, g) metal oleate or methylamine (Figure 1, Method A) or (b, d, f, h) TMSX (Figure 1, Method B). The average edge lengths are shown in the insets.

absorbance and photoluminescence (PL) spectra for these nanocrystals are provided as Supporting Information, Figure S1. The nanocrystals generated from both methods are uniform and have similar sizes and cubic shapes. The TMSI method has a slightly higher yield than the Cs-oleate method, but the PL QY is a bit lower (46% vs 54%). TMSI also needs to be handled more carefully, since it reacts violently with moisture.

CsPbBr<sub>3</sub> Nanocrystals. Compared to CsPbI<sub>3</sub>, CsPbBr<sub>3</sub> has a geometric Goldschmidt tolerance factor that is closer to 1

(0.92 vs 0.89),<sup>49</sup> and the perovskite, γ-orthorhombic phase is the equilibrium structure of CsPbBr<sub>3</sub> at room temperature.<sup>50</sup> This is one reason that perovskite CsPbBr<sub>3</sub> nanocrystals are much more stable than perovskite CsPbI<sub>3</sub> nanocrystals.<sup>51</sup> One common approach to CsPbBr<sub>3</sub> nanocrystal synthesis involves the hot injection of Cs-oleate in ODE into a solution of PbBr<sub>2</sub> dissolved in OA, OAm, and ODE.<sup>3</sup> Compared to CsPbI<sub>3</sub>, the reaction yield is usually a little higher. For example, a typical reaction in 20 mL of ODE produces about 160 mg of CsPbBr<sub>3</sub> nanocrystals, corresponding to 44% molar conversion.

The ionic metathesis reaction shown in eq 3 in Figure 1 results in CsPbBr<sub>3</sub> nanocrystals and Pb-oleate. Other reaction mechanisms are also possible and may be involved as well. One suggestion is that Pb-oleate and oleylammonium bromide (OAm-Br) react with Cs-oleate to form CsPbBr<sub>3</sub> nanocrystals and oleylammonium oleate, <sup>52</sup> as shown in eqs 2a and 2b in Figure 1. Another possibility is the formation of (OAm)<sub>2</sub>PbBr<sub>4</sub> nanosheets as an intermediate species prior to Cs-oleate injection. <sup>53,54</sup> Then, (OAm)<sub>2</sub>PbBr<sub>4</sub> reacts with Cs-oleate to form CsPbBr<sub>3</sub> nanocrystals with possible byproducts like OAm-Br and oleylammonium oleate. Further work is needed to fully verify the mechanistic details of these reactions.

CsPbBr3 nanocrystals can also be synthesized using PbO and NH<sub>4</sub>Br as sources of Pb<sup>2+</sup> and Br<sup>-.55</sup> Cs-oleate is injected into a solution of PbO, NH<sub>4</sub>Br, OA, OAm, and ODE at 180 °C. When trimethylsilyl bromide ((CH<sub>3</sub>)<sub>3</sub>SiBr, TMSBr) is used as the Br source, TMSBr is injected into a mixture of Cs-oleate and Pb-oleate in OAm and ODE at 150 °C. The reaction mechanism is similar to CsPbI3 nanocrystal synthesis using TMSI. TMSBr reacts with OAm to produce OAm-Br, which then reacts with Cs-oleate and Pb-oleate as shown in eq 14 in Figure 1 to produce CsPbBr3 nanocrystals and oleylammonium-oleate as a byproduct. Figure 2c,d shows TEM images of CsPbBr<sub>3</sub> nanocrystals synthesized by hot injection of Cs-oleate or TMSBr. Both reactions produce mostly uniform CsPbBr<sub>3</sub> nanocrystals with a cube shape and a small amount of CsPbBr<sub>3</sub> nanoplatelets. Typical PL QYs are about 50%. The nanocrystals are uniform enough to readily assemble into superlattices. (See Supporting Information Figure S1 for UV-vis absorbance and PL spectra and Figure S2 for additional TEM images.) The reaction kinetics involved in the synthesis of CsPbBr<sub>3</sub> nanocrystals with PbBr<sub>2</sub>, NH<sub>4</sub>Br, or TMSBr are all relatively fast, reaching completion within seconds. The kinetics can be slowed significantly by using 1-bromohexane as the Br source, leading to reactions that take about 20 min to complete. 56 In this approach, a series of chemical transformations takes place, beginning with the formation of CsBr, followed by the formation of Cs<sub>4</sub>PbBr<sub>6</sub> and finally CsPbBr<sub>3</sub>. Questions remain about whether this mechanism also applies to the other halide injection methods with extremely fast reaction kinetics.

CH<sub>3</sub>NH<sub>3</sub>PbI<sub>3</sub> (MAPI) Nanocrystals. Of the metal halides, MAPI nanocrystals are some of the most temperamental and least stable. The synthesis must be carried out at relatively low temperature (55 °C-70 °C) and quenched immediately after reactant injection. The low reaction temperatures are due in part to the volatility of methylamine and methylammonium species.<sup>57</sup> MAPI also decomposes into PbI<sub>2</sub>, NH<sub>3</sub>, and CH<sub>3</sub>I at 75-80 °C.<sup>58</sup>

MAPI nanocrystals are made using the ionic metathesis pathway shown in Figure 1, eq 4. Typical reactions are carried out by adding methylamine in OA to a heated solution of PbI<sub>2</sub> in OA, OAm, and ODE. Methylamine (CH<sub>3</sub>NH<sub>2</sub>) is protonated to methylammonium by OA, and PbI<sub>2</sub> provides

B- and X-site species. <sup>21,59</sup> Since Pb-oleate evolves as a reaction byproduct, PbI<sub>2</sub> must be added in stoichiometric excess relative to CH<sub>3</sub>NH<sub>3</sub>PbI<sub>3</sub>. The molar conversions are usually 60–65%, which is relatively high compared to other perovskite nanocrystals, and a reaction in 10 mL of ODE yields about 70 mg of MAPI nanocrystals.

Methylamine, Pb-oleate, and TMSI can also be used to synthesize MAPI nanocrystals. PbO is dissolved in OA, OAm, and ODE, and then methylamine in THF is added at a reaction temperature of 65 °C, followed immediately by TMSI injection. As described in Figure 1, eq 15, TMSI transforms into OAm-I, which reacts with Pb-oleate, methylamine, and OA to produce MAPI nanocrystals and oleylammonium oleate as a byproduct. Alternatively, benzoyl iodide can be used, reacting in a similar way to TMSI with OA or OAm and releasing HI. Typical reactions, carried out in only 5 mL of ODE, yield about 60 mg of nanocrystals. The PL QYs made using either approach are around 15%. See Supporting Information Figure S1 for absorbance and PL spectra.

Figure 2e,f shows TEM images of MAPI nanocrystals synthesized using PbI<sub>2</sub> or TMSI. Like other metal halide perovskites, MAPI nanocrystals have a cuboidal shape, but the thermodynamically stable phase of MAPI at room temperature is tetragonal, <sup>12,61</sup> which favors increasingly anisotropic growth as the reaction proceeds. <sup>12</sup> MAPI nanocrystals evolve into tetragonal prisms during the reaction. This is one of the challenges to making uniform MAPI nanocrystals: the reaction must be quenched almost immediately, otherwise anisotropic growth takes over and leads to very broad size distributions. <sup>59</sup> TMSI leads to smaller MAPI nanocrystals, but with similar size and shape uniformity.

Double Perovskite Cs<sub>2</sub>AgBiBr<sub>6</sub> Nanocrystals. Cs<sub>2</sub>AgBiBr<sub>6</sub> nanocrystals<sup>62,63</sup> can be made by hot injection of Cs-oleate into a solution of AgBr and BiBr<sub>3</sub> in OA, OAm, and ODE at 200 °C7 or by adding TMSBr to Cs-acetate (CsOOCCH<sub>3</sub>), Bi-acetate (Bi(OOCCH<sub>3</sub>)<sub>3</sub>), and Ag-acetate (AgOOCCH<sub>3</sub>) dissolved in OAm, OA, and ODE at 140 °C.6 TEM images of Cs<sub>2</sub>AgBiBr<sub>6</sub> nanocrystals produced using these two methods are shown in Figure 2g,h. They have a cubic shape, and the TMSBr reaction leads to larger nanocrystals with a broader size distribution. Nucleation and growth is noticeably faster for the TMSBr reaction compared to Csoleate hot injection. The reaction is carried out using Cs-oleate hot injection at 200 °C for 3-5 min, whereas, the TMSBr reaction is carried out for only 10 s at a much lower temperature, 140 °C. The molar conversions of the Cs-oleate and TMSBr reactions are 16% and 25%, respectively. Cs-oleate injection leads to the ionic metathesis reaction shown in eq 5 in Figure 1 to produce Cs2AgBiBr6 nanocrystals and Ag-oleate and Bi-oleate as byproducts. As shown in eqs 8-9 in Figure 1, the TMSBr hot injection reaction involves the transformation of Cs, Bi, and Ag acetate into oleates, which then react directly with TMSBr to produce trimethylsilyl-oleate as a byproduct (Figure 1, eq 17) or TMSBr forms OAm-Br first (Figure 1, eqs 10-12), which then reacts with the metal oleates, which gives oleylammonium oleate as a byproduct (Figure 1, eq 16).

Cs<sub>2</sub>AgBiBr<sub>6</sub> nanocrystals are some of the most stable metal halide perovskite nanocrystals, but the product purity and yields are sensitive to the reaction temperature. Cs-oleate hot injection at 160 °C only produces AgBr and some unidentified compound with an XRD pattern that does not match those of BiBr<sub>3</sub>, CsBr, Cs<sub>3</sub>Bi<sub>2</sub>Br<sub>9</sub>, Cs<sub>3</sub>BiBr<sub>6</sub>, or CsAgBr<sub>2</sub> (see Supporting Information Figure S3 for XRD data). An increase in reaction

temperature from 200 to 225 °C can still give uniform Cs<sub>2</sub>AgBiBr<sub>6</sub> nanocrystals without impurities (Supporting Information Figure S4). When TMSBr injection reactions are carried out at lower temperatures of 120 °C, Cs<sub>2</sub>AgBiBr<sub>6</sub> nanocrystals are produced, but with a significant Cs–Ag–Br byproduct. Hotter reactions, at 180 °C, produce Cs<sub>2</sub>AgBiBr<sub>6</sub> nanocrystals with AgBr contamination.

# ACID AND AMINE: ROLES AND ALTERNATIVES

Figure 3 shows various capping ligands used for metal halide perovskite nanocrystals. Amines are the most common capping

Figure 3. Chemical structures of ligands used in the synthesis of metal halide perovskite nanocrystals. (a–c) Acidic ligands: (a) oleic acid (OA), (b) diisooctylphosphinic acid (DIOP), and (c) tetradecylphosphonic acid (TDPA). (d–f) Basic ligands: (d) oleylamine (OAm), (e) dioctylamine (DOAm), and (f) trioctylphosphine oxide (TOPO). (g–i) Zwitterionic ligands: (g) 3-(N,N-dimethyloctadecylammonio)-propanesulfonate (stearyl sulfobetaine), (h) N-hexadecylphosphocholine (miltefosine), and (i) N,N-dimethyldodecylammoniobutyrate (DDMAB).

ligands. Mixtures of OAm and OA are commonly used. OA can serve as a capping ligand but often plays a direct role as a reactant, as it participates in many ionic metathesis reactions. For example, OA provides the proton source to convert methylamine to the methylammonium cation in the synthesis of MAPI nanocrystals. Without OA, MAPI nanocrystal formation is very slow and results in unstable nanocrystals. The synthesis of CH(NH<sub>2</sub>)<sub>2</sub>PbI<sub>3</sub> (FAPbI<sub>3</sub>) nanocrystals requires a large excess of OA in the preparation of FA-oleate. MAPI and FAPbI<sub>3</sub> nanocrystal synthesis requires OA:OAm mole ratios of at least 4 to 5. Inorganic perovskites employ lower OA:OAm ratios, usually between 1 and 2. The right OA concentration is especially important for optimizing the reaction yield and reproducibility of the synthesis for CsPbBr<sub>3</sub> and Cs<sub>2</sub>AgBiBr<sub>6</sub> nanocrystals.

Amines have been found to be extremely important for the synthesis of metal halide perovskite nanocrystals. The absence

of amines usually leads to bulk crystals.<sup>6</sup> There is one example of CsPbBr<sub>3</sub> nanocrystal synthesis that used only TOPO and OA.<sup>65</sup> Based on <sup>1</sup>H NMR and NOESY data, Cs-oleate serves as the capping ligand in this amine-free synthesis.<sup>65</sup>

Capping ligands on metal halide perovskite nanocrystals tend to desorb in polar solvents, as ligand bonding tends to be ionic.<sup>52</sup> For CsPbBr<sub>3</sub> nanocrystals, both OA and OAm are believed to form X-type ligands (like Cs-oleate, oleylammonium oleate, or oleylammonium bromide). 52,65,66 There are contradicting reports for CsPbI<sub>3</sub> nanocrystals, showing that the capping ligand shell is composed of only OAm<sup>67</sup> or a mixture of OAm and OA.<sup>68</sup> As far as we know, the capping ligand chemistry on MAPI nanocrystals has not yet been reported, so we checked our MAPI nanocrystals using <sup>1</sup>H nuclear magnetic resonance (NMR) spectroscopy and nuclear Overhauser effect spectroscopy (NOESY). We found that both OAm and OA are present in the capping ligand layer (see Supporting Information Figure S5). For Cs<sub>2</sub>AgBiBr<sub>6</sub> nanocrystals, only OAm remains bound to the nanocrystal surface after purification.60

The alkyl chain length <sup>69,70</sup> and the proportion of acid to amine <sup>12,53,60,71</sup> can affect the size and shape of perovskite nanocrystals. CsPbBr<sub>3</sub> nanocrystals obtained from Cs-oleate hot injection reactions at 170 °C in ODE with OAm (Figure 1, eq 3) varied in size from 7 nm to 9 nm to 12 nm when different acids were used: OA, dodecanoic acid, or hexanoic acid (chain lengths of 18, 12, or 6 carbons). <sup>69</sup> In the same study, CsPbBr<sub>3</sub> made with OA and primary amines with hydrocarbon chains shorter than 12 carbons formed nanoplatelets, with thicknesses varying from 4.5 nm to 3.5 nm to 1.8 nm as the chain length decreased from 12 to 8 to 6 carbons. <sup>69</sup> When OA:OAm ratios were changed from 1 to 2 to 4, CsPbBr<sub>3</sub> nanocubes synthesized at 190 °C were found to increase in size from 8 to 10 to 13 nm, while at the same time, the amount of CsPbBr<sub>3</sub> nanoplatelets in the sample increased. <sup>53</sup>

OA and OAm concentrations can also influence the crystal phases produced in a CsPbBr<sub>3</sub> nanocrystal reaction. Increasing the reaction concentrations of both OA and OAm has led to trigonal phase Cs<sub>4</sub>PbBr<sub>6</sub> nanocrystals instead of γ-orthorhombic phase CsPbBr<sub>3</sub> nanocrystals.<sup>53,56</sup> Cs<sub>4</sub>PbBr<sub>6</sub> has attracted attention because of its high PL QY and good stability, although the origin of the luminescence remains under debate.<sup>72–74</sup> Due to highly dynamic ligands and highly mobile halide ions, postsynthetic interconversion between CsPbBr<sub>3</sub> and Cs<sub>4</sub>PbBr<sub>6</sub> nanocrystals can readily occur at room temperature. An excess of amine speeds this transformation by forming soluble molecular species of PbBr<sub>2</sub> that changes CsPbBr<sub>3</sub> to Cs<sub>4</sub>PbBr<sub>6</sub>,<sup>75</sup> which can be reversed by adding OA or PbBr<sub>2</sub> to transform Cs<sub>4</sub>PbBr<sub>6</sub> back to CsPbBr<sub>3</sub>.<sup>76,77</sup>

In some cases, it has been possible to combine OAm with alkyl phosphinic acid or phosphonic acid instead of OA. CsPbI<sub>3</sub> nanocrystals have been synthesized with bis(2,2,4-trimethylpentyl) phosphinic acid (TMPPA).<sup>67</sup> CsPbBr<sub>3</sub> nanocrystals have been made with *n*-tetradecylphosphonic acid (TDPA).<sup>78</sup> And we have made Cs<sub>2</sub>AgBiBr<sub>6</sub> nanocrystals with diisooctylphosphinic acid (DIOP).<sup>60</sup> Figure 4a shows a TEM image of Cs<sub>2</sub>AgBiBr<sub>6</sub> nanocrystals made with DIOP and OAm.

Secondary amines have also been explored as an alternative to OAm. CsPbBr<sub>3</sub> nanocrystals with nearly perfect cube shape and uniformity have been produced using dihexylamine, dioctylamine, didecylamine, didodecylamine, and dioctadecylamine with different sizes of 17, 12, 10, 8, and 7.5 nm. <sup>40</sup> These reactions tend to require more secondary amine than OAm or

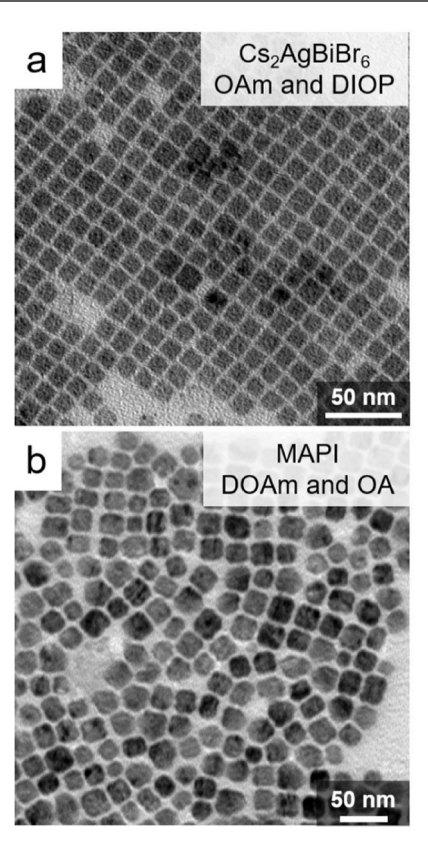


Figure 4. TEM images of (a) Cs<sub>2</sub>AgBiBr<sub>6</sub> nanocrystals synthesized using DIOP and OAm and (b) MAPI nanocrystals synthesized using OA and DOAm.

primary amine because PbBr<sub>2</sub> has a lower solubility in secondary amines. For example, 0.2 mmol (72 mg) of PbBr<sub>2</sub> dissolves in 3 mmol each of OA and octylamine but requires 3 mmol of OA and 5 mmol of dioctylamine for complete dissolution (see Supporting Information Figure S6 for photographs). Secondary amines are also not very effective for perovskites with iodide. Figure 4b shows a TEM image of MAPI nanocrystals that we synthesized with dioctylamine (DOAm) and OA. The nanocrystals have a reasonably narrow size distribution; however, colloidal stability is poor, and they exhibit very low PL QYs of only 1% (see Figure S7 in Supporting Information for XRD, UV—vis absorbance, and PL spectra). CsPbI<sub>3</sub> nanocrystals synthesized using secondary amines have been reported to degrade rapidly into the yellow phase, within only a few hours.<sup>40</sup>

The zwitterionic ligands shown in Figure 3, including stearyl sulfobetaine, miltefosine, and DDMAB, have also been used to make  $CsPbX_3$  (X=Cl,Br,I) nanocrystals. Sulfobetaine-capped  $CsPbBr_3$  nanocrystals have been reported to have higher stability compared to OA/OAm-capped nanocrystals. Sulfobetaine-capped nanocrystals purified by precipitation with ethyl acetate and stored under ambient conditions for 28 days were shown to retain PL QYs of ~75%, while the PL QY of their OA/OAm-capped nanocrystals dropped to 20%.

# REACTION TEMPERATURE, TIME, AND QUENCHING

Several factors determine the appropriate reaction temperature and time, including reactant solubility, particle nucleation and growth rates, and thermal stability of the perovskite phase. Figure 5 shows examples of undesirable phase transformations

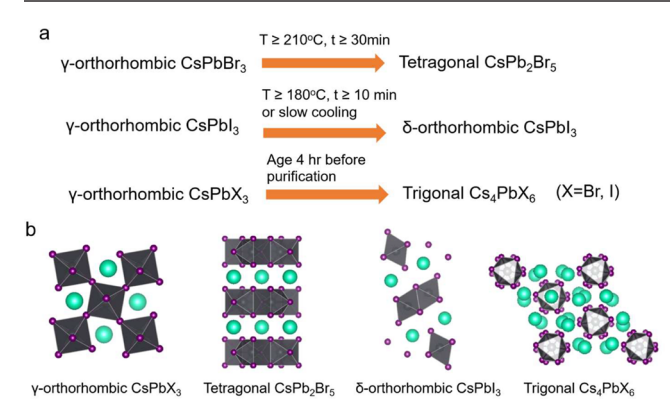


**Figure 5.** (a) Undesirable phase transformations occur when CsPbX<sub>3</sub> (X = Br, I) nanocrystals are not handled properly during synthesis and purification. Several examples of transformations from the  $\gamma$ -orthorhombic perovskite phase to nonperovskite phases are shown. <sup>80–82</sup> The temperature, T, is the hot injection temperature, and time, t, is duration of the reaction after hot injection. (b) Perovskite  $\gamma$ -orthorhombic CsPbX<sub>3</sub> crystal structure shown in comparison with the nonperovskite crystal structures of tetragonal CsPb<sub>2</sub>Br<sub>5</sub>,  $\delta$ -orthorhombic CsPbI<sub>3</sub>, and trigonal Cs<sub>4</sub>PbX<sub>6</sub>.

that can occur for  $CsPbX_3$  (X = Cl, Br, I) nanocrystals during synthesis and purification. In some cases, unwanted materials can form. For example, when the synthesis of CsPbBr3 and CsPbCl<sub>3</sub> nanocrystals is carried out at 260 °C—which is too hot—the reaction produces CsPb<sub>2</sub>Br<sub>5</sub> and CsPb<sub>2</sub>Cl<sub>5</sub>.80 When the reaction temperature for CsPbBr3 nanocrystals is lower than 140 °C, CsPbBr3 nanoplatelets form instead of nanocubes.<sup>53</sup> For CsPbI<sub>3</sub>, excessive reaction temperatures produce bulk crystals of the yellow nonperovskite,  $\delta$ -orthorhombic phase.<sup>81</sup> There are some cases in which reactions can be performed at higher temperatures by modifying reactant concentrations. CsPbX<sub>3</sub> nanocrystals can be grown at relatively high temperatures of 250-260 °C by adding OAm-X to the reaction mixture prior to Cs-oleate injection. 80,81 For MAPI nanocrystals, reaction temperatures higher than 100 °C induce anisotropic particle growth and the formation of platelets instead of nanocubes. 12 Cs2AgBiBr6 nanocrystals are usually made by Cs-oleate hot injection at 200 °C, but we have found that reactions at 225 °C also work to produce uniform Cs<sub>2</sub>AgBiBr<sub>6</sub> nanocrystals (see Supporting Information Figure S4 for TEM images). Reactions at much lower temperatures, e.g., 160 °C, only produce AgBr and other binary or tertiary Br-containing impurities.

Some reactants precipitate when the solution temperature is too high. CsPbI $_3$  nanocrystal synthesis is usually performed below 185 °C to avoid precipitation of PbI $_2$  from OAm, OA, and ODE solutions. PbBr $_2$  is more soluble than PbI $_2$  at higher temperatures, which enables reactions up to about 200–210 °C for the synthesis of CsPbBr $_3$  nanocrystals. The solubility of PbX $_2$  does also depend somewhat on ligand concentration, and reaction temperatures can be raised by adding more OA or OAm to the ODE reaction solution. S3,83

Most metal halide perovskite nanocrystals are also very sensitive to the reaction time because of their fast nucleation and growth kinetics. The synthesis of CsPbX<sub>3</sub> and MAPI nanocrystals is completed in less than 10 s.<sup>3,59</sup> To prevent unwanted growth and aggregation, the reactions must be quenched by immersion in an ice water bath. CsPbBr<sub>3</sub> nanocrystal reactions at 150 °C prolonged for 30–90 min produce CsPbBr<sub>3</sub> nanowires.<sup>84</sup> Reactions at 210 °C for 30 min

result in CsPb<sub>2</sub>Br<sub>5</sub> (see Supporting Information Figure S8 for XRD and TEM data). CsPbI<sub>3</sub> nanocrystal reactions at 180 °C carried out for 5–10 min yield yellow  $\delta$ -orthorhombic phase nanowires. Reactions must be immediately quenched to obtain the metastable black perovskite phase of CsPbI<sub>3</sub>. Slow cooling always yields yellow,  $\delta$ -orthorhombic CsPbI<sub>3</sub> nanocrystals (see Supporting Information Figure S9 for TEM images). In TEM images 1.

The amount of time spent between reaction and purification can also be very important.  $CsPbI_3$  nanocrystals should be isolated immediately from crude reaction mixtures to prevent transformation to the yellow phase. After several hours without purification,  $CsPbI_3$  nanocrystals (sealed under  $N_2$ ) change from cubes to polyhedra (see Supporting Information Figure S9). In this case, excess ligand in the crude reaction mixture probably promotes the transformation  $CsPbI_3$  nanocrystals into  $Cs_4PbI_6$ —a process that has actually been exploited to intentionally change  $CsPbX_3$  (X = Br, I) nanocrystals into  $Cs_4PbX_6$ .  $^{76,82}$ 

#### PURIFICATION

Early synthetic work relied on high speed centrifugation to collect and purify nanocrystals from crude reaction mixtures in order to prevent degradation.  $^{11,12,44,45}$  For example, researchers showed that precipitative washing with antisolvents significantly decreased the PL QY of CsPbBr3 nanocrystals from 60 to 70% to just 8–10%,  $^{30,87}$  and destroyed black, perovskite-phase CsPbI3 nanocrystals by promoting aggregation, changes in size, and a reversion to the yellow  $\delta$ -orthorhombic phase by aggregation. But high speed antisolvent-free centrifugation leaves a significant amount of nanocrystals suspended in the supernatant. These nanocrystals are discarded, significantly lowering the product yields, and a substantial amount of unbound ligand and residual ODE ends up in the product.  $^{30,32,52,89}$ 

These days, antisolvents are used more frequently, although standard protocols for precipitative purification of metal halide perovskite nanocrystals are still being refined. Pigure 6 shows data from our laboratory comparing CsPbBr<sub>3</sub>, CsPbI<sub>3</sub>, and MAPI nanocrystals that were either isolated without antisolvent or precipitated with methyl acetate. The amount of material collected using methyl acetate is much higher, and the absorbance and PL spectra are largely unchanged. The PL QY of CsPbBr<sub>3</sub> nanocrystals decreased slightly from 74% to 54%; the CsPbI<sub>3</sub> nanocrystals are actually brighter (up to 54% from 41%), and MAPI nanocrystals have PL QYs of 15%, regardless of whether methyl acetate was used or not.

One source of uncertainty regarding the effectiveness of antisolvent precipitation in the literature is the absence of important experimental details like solvent:antisolvent volume ratio, centrifuge speed, and time. 30,32,43,88,90 Subtle variations in the precipitation methods matter. For this perspective, we tested methanol, 1-butanol, acetonitrile, acetone, methyl acetate, and ethyl acetate on CsPbBr<sub>3</sub>, CsPbI<sub>3</sub>, MAPI, and Cs<sub>2</sub>AgBiBr<sub>6</sub> nanocrystals using a set of normalized conditions of solvent-to-antisolvent ratio and centrifugation speed and time, to determine which combinations of antisolvents and nanocrystals are viable. The results are shown in Table 1, and additional TEM images are provided as Supporting Information Figures S11–S14. CsPbBr<sub>3</sub> nanocrystals are compatible with all six antisolvents, although there is a slight variation in the uniformity of the nanocrystals obtained after purification. Cs<sub>2</sub>AgBiBr<sub>6</sub> is incompatible only with methanol. And CsPbI<sub>3</sub>

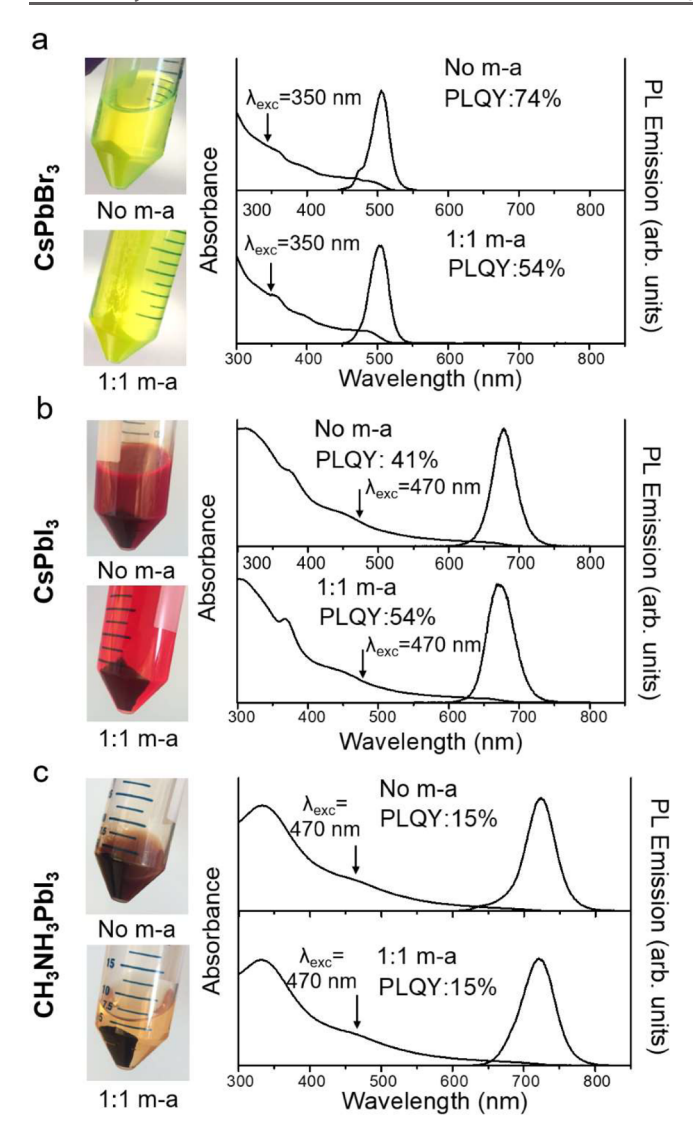


**Figure 6.** Photos of centrifuge tubes after precipitation of the nanocrystals from the crude reaction product and UV—vis absorbance and photoluminescence (PL) emission spectra of redispersed (a) CsPbBr<sub>3</sub>, (b) CsPbI<sub>3</sub>, and (c) MAPI nanocrystals. The nanocrystals in the photos were precipitated by centrifugation under the same conditions (8000 rpm or 8228 × g, 5 min) either without antisolvent or with the addition of an equivalent volume of methyl acetate (m-a) to the crude reaction mixture. Additional precipitations caused the nanocrystals to aggregate. The excitation wavelength ( $\lambda_{\rm exc}$ ) is shown in each plot, and PL QYs were determined relative to Rhodamine B.

and MAPI nanocrystals are degraded by both methanol and acetone.

Figure 7 shows more data for CsPbBr<sub>3</sub> and CsPbI<sub>3</sub> nanocrystals isolated by various precipitation methods. CsPbBr<sub>3</sub> nanocrystals precipitated with methanol or acetonitrile had PL QYs greater than 90%, methyl acetate and ethyl acetate led to slightly lower PL QYs of 68% and 65%, and acetone yielded nanocrystals with the lowest PL QY of 56%. In the PL spectra in Figure 7b for CsPbBr<sub>3</sub> nanocrystals precipitated with the different antisolvents, the sample obtained with methanol exhibited the narrowest and most symmetric line width, which is consistent with the monodisperse morphology of nanocubes observed by TEM (Supporting Information, Figures S11). The PL peak was slightly red-shifted compared to the others, probably because

Table 1. Antisolvent Compatibility of CsPbBr<sub>3</sub>, CsPbI<sub>3</sub>, MAPI, and Cs<sub>2</sub>AgBiBr<sub>6</sub> Nanocrystals<sup>a</sup>

	CsPbBr <sub>3</sub>	$CsPbI_3$	MAPI	$Cs_2AgBiBr_6$
methanol	$\checkmark$	×	×	×
1-butanol	$\sqrt{}$	$\sqrt{}$	$\sqrt{}$	$\checkmark$
acetone	$\checkmark$	×	×	$\sqrt{}$
acetonitrile	$\checkmark$	$\sqrt{}$	$\sqrt{}$	$\sqrt{}$
methyl acetate	$\checkmark$	$\sqrt{}$	$\sqrt{}$	$\sqrt{}$
ethyl acetate	$\checkmark$	$\sqrt{}$	$\sqrt{}$	$\sqrt{}$

a The crude reaction product from a single reaction was divided into six centrifuge tubes, and an equal volume of antisolvent was added to each. Samples were centrifuged at 8000 rpm (8228 × g) for 5 min. The precipitated nanocrystals were redispersed in 5 mL of hexane and centrifuged again at 8500 rpm (9289 × g) for 5 min to remove all solid byproducts, including poorly capped nanocrystals. Compatible ( $\sqrt{}$ ) means that the antisolvent does not affect the crystal structure, morphology, or optical properties and that the nanocrystals redisperse in hexane. Incompatible (×) means that the antisolvent causes the nanocrystals to aggregate or exhibit degraded properties. (Additional photographs of the centrifuge tubes, TEM images, and optical data are provided as Supporting Information Figures S10−S16).

methanol is not soluble with ODE and, as a result, only precipitates a small portion of the largest nanocrystals in the sample, effectively resulting in a size-selective precipitation. The PL spectra for the other CsPbBr<sub>3</sub> nanocrystals are more asymmetric, with a shorter-wavelength shoulder. These spectra are also consistent with the TEM-observed sample morphologies—i.e., a mixture of nanoplatelets and nanocubes that are more consistent with the as-synthesized product. CsPbI<sub>3</sub> nanocrystals precipitated with 1-butanol, acetonitrile, methyl acetate, and ethyl acetate exhibited PL QYs of 33%, 60%, 54%, and 52%. As shown in Figure 7c, the PL peaks of these four samples are very similar, but the peak maximum for CsPbI<sub>3</sub> nanocrystals precipitated with methyl acetate is slightly blueshifted compared to the others.

In some cases, antisolvents are clearly not compatible. Methanol and acetone have no obvious effect on CsPbBr<sub>3</sub> nanocrystals but change the color of the CsPbI<sub>3</sub> and MAPI nanocrystals to pale-yellow materials, as shown in Figure 7a. This is because CsPbI<sub>3</sub> has reverted to its equilibrium yellow, nonperovskite phase and MAPI has degraded into PbI<sub>2</sub>. In other cases, solvent degradation is less obvious. For example, Cs<sub>2</sub>AgBiBr<sub>6</sub> nanocrystals precipitated with methanol do not change color, but they cannot be redispersed. Antisolvents can sometimes change the nanocrystal morphology. CsPbI<sub>3</sub> nanocrystals precipitated with 1-butanol exhibit reasonably high PL QYs of 33%, but TEM showed a change in shape from cubes to nanorods. (See Supporting Information Figure S12 for TEM images.)

In addition to the solvent:antisolvent volume ratio and centrifuge speed and time, we encourage reporting of additional purification details that we have found to be important, including the concentration and volume of the crude reaction solution, if the solvents and antisolvents need to be anhydrous, <sup>92</sup> if the use of glovebox is necessary, if low temperature centrifugation is helpful, if vortexing or even sonication is needed to redisperse the precipitate, and if the waiting time between centrifuge cycles matters.

Purification procedures can be especially important for some analyses. For example, NMR spectroscopy studies of ligand bonding are especially sensitive to free ligand, and these studies require nanocrystals that have been precipitated and

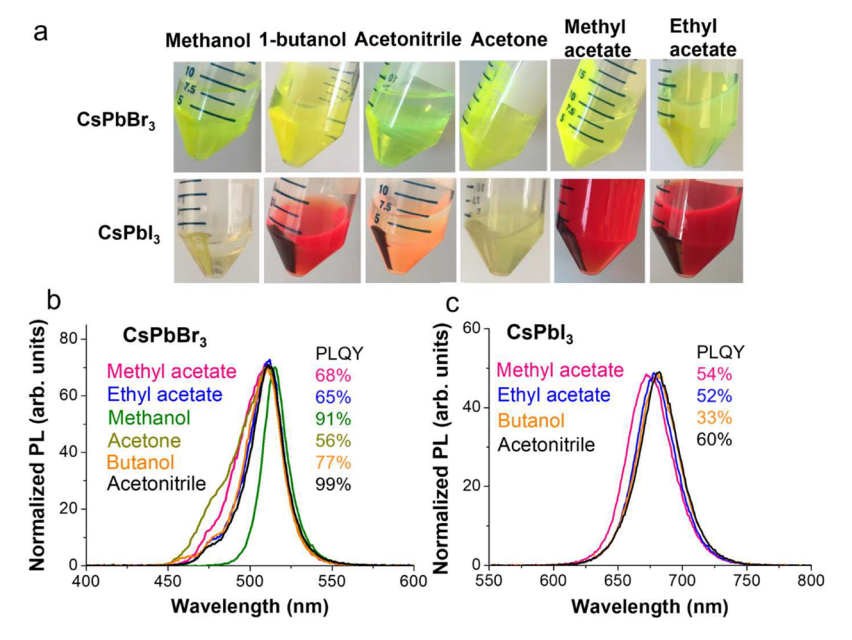


Figure 7. Solvent/antisolvent purification of CsPbBr<sub>3</sub> and CsPbI<sub>3</sub> nanocrystals. Nanocrystals were dispersed in ODE and mixed with 1:1 (v:v) methanol, 1-butanol, acetonitrile, acetone, methyl acetate, or ethyl acetate and then centrifuged. (a) Photographs of the centrifuge tubes after centrifugation. The solvent polarity decreases from left to right. None of the solvents lead to a color change for CsPbBr<sub>3</sub> nanocrystals. CsPbI<sub>3</sub> nanocrystals changed from dark red to pale yellow when methanol and acetone were used. There was no color change with 1-butanol, acetonitrile, methyl acetate, and ethyl acetate, although the supernatant obtained with acetonitrile had an orange-pink color. The supernatants obtained with methanol and acetonitrile exhibited a liquid—liquid phase separation. (See Supporting Information, Figure S10 for photographs of the phase separation). PL spectra are shown for (b) CsPbBr<sub>3</sub> ( $\lambda_{exc}$  = 350 nm) and (c) CsPbI<sub>3</sub> ( $\lambda_{exc}$  = 470 nm) nanocrystals purified with the antisolvents that did not lead to immediate degradation. PL QYs were determined relative to Rhodamine B.

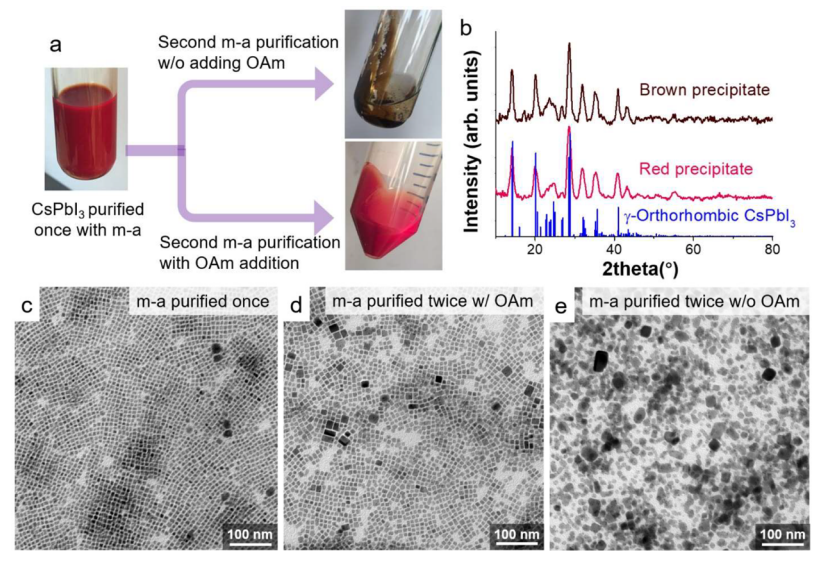


Figure 8. Effect of a second antisolvent precipitation step on CsPbI<sub>3</sub> nanocrystals. Nanocrystals were dispersed in 3 mL of hexane and then centrifuged at 8000 rpm (8228 × g) for 3 min after adding 3 mL of methyl acetate. (a) CsPbI<sub>3</sub> nanocrystals obtained with and without the addition of 5 μL of OAm prior to adding methyl acetate. (b) XRD of the nanocrystal precipitates shown in (a). Both patterns match the black perovskite, γ-orthorhombic phase of CsPbI<sub>3</sub>.  $^{21,39}$  (c–e) TEM images of CsPbI<sub>3</sub> nanocrystals (c) purified once with m-a, (d) purified twice with m-a with OAm addition, and (e) purified twice with m-a without OAm addition.

redispersed at least twice during the purification process. This can be especially challenging for metal halide perovskite nanocrystals. Figure 8a shows data for CsPbI<sub>3</sub> nanocrystals that illustrates this challenge. CsPbI<sub>3</sub> nanocrystals obtained after a second precipitative wash (1:1 (v:v) methyl acetate:hexane) have lost their bright red color and could not be redispersed in hexane. The brown color is still consistent with perovskite-phase nanocrystals—i.e., they have not reverted to the yellow

phase, as the XRD in Figure 8b confirms—but are no longer luminescent and have lost some of their distinct cubic shape. The beautiful red color of CsPbI $_3$  nanocrystal dispersions and films comes from their bright luminescence. The inability to redisperse the nanocrystals signals that much of the ligand shell has been lost. We found that the addition of OAm to the nanocrystal dispersion (5–10  $\mu$ L of OAm to 3 mL of nanocrystal dispersion with a concentration of 5–10 mg/mL)

before the second methyl acetate precipitation can be used to obtain fluorescent, redispersible CsPbI<sub>3</sub> nanocrystals essentially free of unbound ligand (see Supporting Information Figure S17 for NMR spectra). Figure 8b-e shows XRD and TEM images. The nanocrystals are easily dried. Beware, however, because OAm addition prior to a second precipitative washing can also degrade some materials. Cs2AgBiBr6 nanocrystals, for example, decompose in the presence of excess amine to Cs-Bi-Br compounds and Ag nanocrystals. Also, some nanocrystals are so sensitive to antisolvent that they must first be collected by antisolvent-free centrifugation and then precipitated using solvent/antisolvent techniques. We found this to be true for dioctylamine-capped MAPI nanocrystals. In that process, some material is lost during the initial antisolvent-free isolation step, but the final product obtained after antisolvent precipitation is free of contaminants and is not degraded.

After isolating the nanocrystals, they should generally be stored as concentrated dispersions. Nanocrystals stored as a dry powder are much more susceptible to degradation than dispersions. Most metal halide perovskite nanocrystals are also sensitive to oxygen, moisture, and light, and we have found that nanocrystals remain most stable when dispersed in nonpolar solvents like hexane or toluene, sealed under inert atmosphere, wrapped with aluminum foil, and stored in a refrigerator. Many different techniques have been used to track the stability of metal halide perovskite nanocrystals, including XRD, TEM, dynamic light scattering, Fourier transform infrared (FTIR) spectroscopy, and PL QY measurements.

There are a number of ongoing efforts to develop more effective postsynthetic surface treatments to passivate surface defects and improve the stability of perovskite nanocrystals. P2,95-102 A wide range of surface-passivating agents have been tried on CsPbBr3 and/or CsPbI3 nanocrystals, including quaternary ammonium bromides, octylphosphonic acid, hexylphosphonate, trioctylphosphine, tri-n-butylphosphine, bidentate ligands like 2,2'-iminodibenzoic acid, and sodium or ammonium salts like sodium thiocyanate (NaSCN) or sodium tetrafluoroborate (NaBF4). These treatments have enhanced colloidal stability and photostability and shown improvements in the PL QYs of CsPbBr3 and/or CsPbI3 nanocrystals, with some having reached nearly 100% PL QY. Less has been done with hybrid organic—inorganic perovskite (HOIP) nanocrystals and lead-free double perovskite nanocrystals.

## ■ TEM SAMPLE PREPARATION AND IMAGING

For TEM imaging,  $CsPbI_3$  and MAPI nanocrystals should be imaged as soon as possible after being deposited and dried on a TEM grid. These nanocrystals degrade quickly in air—within a few hours. Figure 9a,b shows  $CsPbI_3$  and MAPI nanocrystals that were imaged 5 h after preparing the TEM grids. The large, circular nanocrystals in Figure 9a are mostly  $\delta$ -orthorhombic phase  $CsPbI_3$ , and the MAPI nanocrystals in Figure 9b are largely rod- and wire-shaped, which signals the formation of hydrated MAPI<sup>103</sup> and the decomposition product,  $PbI_2$ . In comparison, TEM imaging of  $CsPbBr_3$  and  $Cs_2AgBiBr_6$  nanocrystals tends to be easier because samples on TEM grids are relatively stable in air and can be imaged without losing their morphology or degrading for several days. We have been able to image a few samples even months after depositing them on a TEM grid.

For studying superlattices, it is important to understand the stability of the nanocrystals. To prepare nanocrystal super-

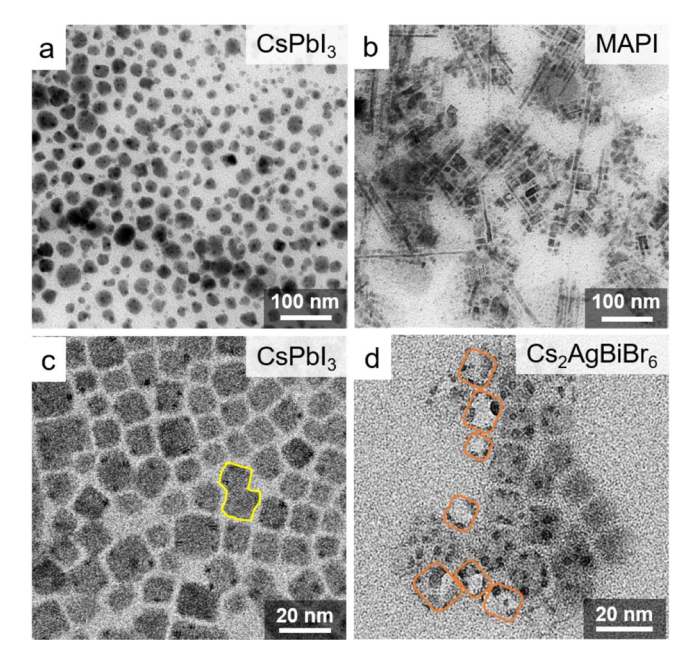


**Figure 9.** TEM images of degraded (a) CsPbI<sub>3</sub>, (b) MAPI, (c) CsPbI<sub>3</sub> and (d) Cs<sub>2</sub>AgBiBr<sub>6</sub> nanocrystals. The (a) CsPbI<sub>3</sub> and (b) MAPI nanocrystals had been left out in air at 50% relative humidity for 5 h before imaging, and the (c) CsPbI<sub>3</sub> and (d) Cs<sub>2</sub>AgBiBr<sub>6</sub> nanocrystals were imaged immediately after preparing the samples. The degradation in (c) and (d) are due to the effects of the electron beam. In (c), domains are highlighted in yellow of two neighboring nanocrystals coalescing. In (d), the regions highlighted in orange are the initial locations of Cs<sub>2</sub>AgBiBr<sub>6</sub> nanocrystals that have evaporated under the beam and small Ag nanoparticles have formed. All images were acquired on a JEOL 2010F TEM at 200 kV.

lattices for TEM imaging, we often place a TEM grid flat on the bottom of a vial, immersed in a concentrated dispersion, and let the solvent evaporate overnight. For most metal halide perovskite nanocrystals, this needs to be done in a glovebox or under inert atmosphere to retain the integrity of the nanocrystals.<sup>21,59</sup>

High resolution TEM or scanning transmission electron microscopy (STEM) imaging often requires additional treatment of the TEM samples to remove excess ligands. Heating the TEM grid under vacuum can remove excess ligand, but this rapidly degrades the nanocrystals and induces unwanted growth and aggregation. We tend to briefly dip the grid into methyl acetate for about 1 s and image the sample as soon as possible. After the dip, the nanocrystals are even more susceptible to degradation in air and moisture. To further reduce carbon contamination, the grid can be loaded into the TEM and left under vacuum for a few hours with the beam turned off.

Metal halide perovskite nanocrystals are also sensitive to beam damage. <sup>105,106</sup> The beam induces the formation of high-contrast spots near the edges and corners of the nanocrystals, as shown for example in Figure 9c,d for CsPbI<sub>3</sub> and Cs<sub>2</sub>AgBiBr<sub>6</sub>. These high contrast spots are Pb<sup>0</sup> in the case of CsPbX<sub>3</sub> nanocrystals—the result of beam-induced reduction of Pb<sup>2+</sup> to Pb<sup>0</sup> and volatilization of the halogen species. <sup>106</sup> Similarly, Ag nanoparticles form at the surfaces of Cs<sub>2</sub>AgBiBr<sub>6</sub> nanocrystals. <sup>7</sup> Sometimes, the beam induces coalescence of neighboring nanocrystals. An example of this is highlighted in Figure 9c. Sometimes this beam-induced coalescence does not degrade the nanocrystals; for example, CsPbBr<sub>3</sub> nanocrystals

have been observed to coalesce without any change in elemental composition or electronic structure. Osometimes the beam will completely destroy the nanocrystals. Osometimes the beam will completely destroy the nanocrystals. Osometimes in Figure 9d, some of the Cs<sub>2</sub>AgBiBr<sub>6</sub> nanocrystal cores have disappeared, leaving only a few Ag particles behind. Hybrid organic—inorganic perovskites (HOIP) especially suffer from decomposition under the beam; for example, MAPI decomposes into PbI<sub>2</sub>. Osomethic degradation due to the beam, including dose minimization, osomethic in-line holography, of and cryo-EM, osomethic degradation due to the beam, including dose minimization, osomethic in-line holography, osomethic degradation due to the beam, including dose minimization, osomethic in-line holography, osomethic degradation due to the beam, including dose minimization, osomethic in-line holography, osomethic degradation due to the beam, including dose minimization, osomethic in-line holography, osomethic degradation due to the beam, including dose minimization, osomethic degradation due to the beam, including dose minimization, osomethic degradation due to the beam, including dose minimization, osomethic degradation due to the beam, including dose minimization, osomethic degradation due to the beam, including dose minimization, osomethic degradation due to the beam, including dose minimization, osomethic degradation due to the beam.

#### CONCLUSIONS

The synthesis of uniform, dispersible metal halide perovskite nanocrystals with high quality optical properties requires the control of reactant concentrations, reaction temperatures, and time. For CsPbI3 nanocrystals, for example, the reaction temperature, time, and quenching need to be carefully controlled in order to trap the desired, metastable perovskite phase. Some reactions happen very quickly, but not in all cases. Most syntheses involve metathesis reactions and amines especially OAm—as capping ligands. Purification can be accomplished by antisolvent precipitation strategies, but the antisolvent chemistry and separation procedures have required a significant amount of optimization compared to other types of nanocrystals due to the relatively labile, ionic bonding of the capping ligands to the metal halide surface. We have tried to show some of the benefits of using antisolvent precipitation to isolate nanocrystals compared to "antisolvent-free" separations. We finally discussed some of the practical issues that face TEM characterization of metal halide perovskite nanocrystals, which include air sensitivity of TEM samples and electron beam damage. We hope that this perspective helps explain and resolve some of the known troubles that researchers have encountered when working with metal halide perovskite nanocrystals. In the end, we encourage researchers to report (and discuss) more of the seemingly trivial experimental details in their papers—which have turned out not to be so trivial.

## ASSOCIATED CONTENT

#### Supporting Information

The Supporting Information is available free of charge at https://pubs.acs.org/doi/10.1021/acs.chemmater.0c01735.

Experimental details; UV-vis absorbance and PL spectra of CsPbI<sub>3</sub>, CsPbBr<sub>3</sub>, and MAPI nanocrystals synthesized using different methods; additional TEM images of CsPbBr<sub>3</sub> nanocubes with a few nanoplatelets; XRD of Cs<sub>2</sub>AgBiBr<sub>6</sub> nanocrystals synthesized at 160 °C; TEM of Cs<sub>2</sub>AgBiBr<sub>6</sub> nanocrystals synthesized at 225 °C; <sup>1</sup>H NMR and NOESY of MAPI nanocrystals synthesized with oleic acid and oleylamine; photographs of PbBr<sub>2</sub> dissolved in dioctylamine or octylamine; XRD, absorbance, and PL spectra of MAPI nanocrystals synthesized using oleic acid and dioctylamine; TEM and XRD of CsPbBr3 nanocrystals reacting at 210 °C for different times; TEM of the  $\delta$ -orthorhombic phase CsPbI<sub>3</sub> nanorods and trigonal phase Cs<sub>4</sub>PbI<sub>6</sub> nanocrystals; photographs of centrifuge tubes of MAPI and Cs<sub>2</sub>AgBiBr<sub>6</sub> nanocrystals purified with different antisolvents; TEM images of CsPbBr<sub>3</sub>, CsPbI<sub>3</sub>, MAPI, and Cs<sub>2</sub>AgBiBr nanocrystals purified with different antisolvents; photograph of 1-butanol purified CsPbI<sub>3</sub> nanocrystals; PL spectra of MAPI nanocrystals purified with different antisolvents; and <sup>1</sup>H NMR of CsPbI<sub>3</sub> nanocrystals purified twice with methyl-acetate and with oleylamine addition between the two cycles (PDF)

#### AUTHOR INFORMATION

#### **Corresponding Author**

Brian A. Korgel — McKetta Department of Chemical Engineering and Texas Materials Institute, The University of Texas at Austin, Austin, Texas 78712-1062, United States; orcid.org/0000-0001-6242-7526; Email: korgel@che.utexas.edu

#### **Authors**

Yangning Zhang — McKetta Department of Chemical Engineering and Texas Materials Institute, The University of Texas at Austin, Austin, Texas 78712-1062, United States; orcid.org/0000-0001-5511-955X

Timothy D. Siegler – McKetta Department of Chemical Engineering and Texas Materials Institute, The University of Texas at Austin, Austin, Texas 78712-1062, United States; orcid.org/0000-0001-6033-2232

Cherrelle J. Thomas – McKetta Department of Chemical Engineering and Texas Materials Institute, The University of Texas at Austin, Austin, Texas 78712-1062, United States

Michael K. Abney – McKetta Department of Chemical Engineering and Texas Materials Institute, The University of Texas at Austin, Austin, Texas 78712-1062, United States

**Tushti Shah** – McKetta Department of Chemical Engineering and Texas Materials Institute, The University of Texas at Austin, Austin, Texas 78712-1062, United States

Anastacia De Gorostiza — McKetta Department of Chemical Engineering and Texas Materials Institute, The University of Texas at Austin, Austin, Texas 78712-1062, United States

Randalynn M. Greene – McKetta Department of Chemical Engineering and Texas Materials Institute, The University of Texas at Austin, Austin, Texas 78712-1062, United States

Complete contact information is available at: https://pubs.acs.org/10.1021/acs.chemmater.0c01735

#### Notes

The authors declare no competing financial interest.

#### **Biographies**

Yangning Zhang received her B.S. in Chemical Engineering from Tianjin University in China in 2016. She is currently a Ph.D. candidate in Chemical Engineering in the Korgel Group at the University of Texas at Austin (UT Austin). Her research focuses on metal halide perovskite nanocrystals and understanding their surfaces, stability, optical properties, and superlattice assembly.

Dr. Timothy D. Siegler received his B.S. in Chemical Engineering from the University of Notre Dame in 2014 and his Ph.D. in Chemical Engineering from UT Austin in 2019. His work has focused on understanding the stability of halide perovskite and metal halide films under humid conditions, the development of tandem perovskite solar cell architectures, and the synthesis of halide perovskite and elpasolite nanocrystals. He is currently a postdoctoral fellow at the University of Washington.

Dr. Cherrelle J. Thomas received her B.S. in Chemical Engineering at Howard University in 2013 and her Ph.D. in Chemical Engineering from UT Austin in 2018. Her research has focused on surface

functionalization of  ${\rm CuInSe_2}$  and  ${\rm CsPbI_3}$  nanocrystals and their effect on conversion yields, exciton kinetics, and thermal stability. She is now a postdoctoral fellow at Sandia National Laboratories in Albuquerque, NM.

Michael K. Abney received his B.S. in Chemical Engineering from the University of Kentucky in 2011. He then worked for 5 years at the Marathon Petroleum Corporation and Keystone Engineering. He is a Ph.D. candidate in Chemical Engineering at UT Austin in the Korgel Group. His research focuses on the optical and electronic properties of inorganic perovskite nanocrystals and their application in photovoltaic devices.

Tushti Shah received her B.S. degree in Chemical Engineering from the Indian Institute of Technology—Gandhinagar. She is a Ph.D. student in Chemical Engineering at UT Austin in the Korgel Group. She focuses on the synthesis, surface chemistry, and optical properties of silicon and germanium nanomaterials and understanding their stability under different environmental conditions. She has also developed various high resolution TEM and STEM imaging and electron energy loss spectroscopy (EELS) methods for nanocrystal materials.

Anastacia De Gorostiza is a first year B.S. Chemical Engineering student at UT Austin. She is currently a research assistant in the Korgel Group focusing on the study of metal halide perovskite nanocrystals and their optical and physical properties.

Randalynn M. Greene received her B.S. degree in Chemical Engineering from UT Austin in 2019. In addition to working on metal halide perovskites as an undergraduate researcher in the Korgel Group, she helped develop the synthesis of CuInSe<sub>2</sub>, GeTe, and GeSbTe nanocrystals. She will be a Ph.D. student in Chemical Engineering at Iowa State University beginning in Fall, 2020.

Professor Brian A. Korgel is the Ernest J. Cockrell, Jr. Memorial Chair in Engineering at UT Austin. He directs the Industry/University Research Center (IUCRC) for Next Generation Photovoltaics and the Emerging Technologies area of the UTlPortugal program and serves as the Education and Outreach Director for the UT Austin MRSEC. He works on nano & mesoscopic materials chemistry and complex fluids, tackling problems in lighting, data storage and processing, wearables, energy storage, chemical transformations, energy harvesting and conversion, and medicine. He is also an artist, exploring collaboration, language, and human-artificial intelligence/robot cohabitation.

## ACKNOWLEDGMENTS

Financial support of this work was provided by the Robert A. Welch Foundation (F-1464), the Industry/University Cooperative Research Center on Next Generation Photovoltaics (IIP-1540028), the UTlPortugal program, and the Center for Dynamics and Control of Materials (CDCM) Materials Research Science and Engineering Center (MRSEC) (DMR-1720595).

## **■** REFERENCES

- (1) Kovalenko, M. V.; Protesescu, L.; Bodnarchuk, M. I. Properties and Potential Optoelectronic Applications of Lead Halide Perovskite Nanocrystals. *Science* **2017**, *358*, 745–750.
- (2) Akkerman, Q. A.; Manna, L. What Defines a Halide Perovskite? ACS Energy Lett. 2020, 5, 604-610.
- (3) Protesescu, L.; Yakunin, S.; Bodnarchuk, M. I.; Krieg, F.; Caputo, R.; Hendon, C. H.; Yang, R. X.; Walsh, A.; Kovalenko, M. V. Nanocrystals of Cesium Lead Halide Perovskites (CsPbX<sub>3</sub>, X = Cl, Br,

- and I): Novel Optoelectronic Materials Showing Bright Emission with Wide Color Gamut. *Nano Lett.* **2015**, *15*, 3692–3696.
- (4) Sun, S.; Yuan, D.; Xu, Y.; Wang, A.; Deng, Z. Ligand-Mediated Synthesis of Shape-Controlled Cesium Lead Halide Perovskite Nanocrystals via Reprecipitation Process at Room Temperature. *ACS Nano* **2016**, *10*, 3648–3657.
- (5) Xiao, J. W.; Liang, Y.; Zhang, S.; Zhao, Y.; Li, Y.; Chen, Q. Stabilizing RbPbBr<sub>3</sub> Perovskite Nanocrystals through Cs<sup>+</sup> Substitution. *Chem. Eur. J.* **2018**, *25*, 2597–2603.
- (6) Creutz, S. E.; Crites, E. N.; De Siena, M. C.; Gamelin, D. R. Colloidal Nanocrystals of Lead-Free Double-Perovskite (Elpasolite) Semiconductors: Synthesis and Anion Exchange To Access New Materials. *Nano Lett.* **2018**, *18*, 1118–1123.
- (7) Bekenstein, Y.; Dahl, J. C.; Huang, J.; Osowiecki, W. T.; Swabeck, J. K.; Chan, E. M.; Yang, P.; Alivisatos, A. P. The Making and Breaking of Lead-Free Double Perovskite Nanocrystals of Cesium Silver Bismuth Halide Compositions. *Nano Lett.* **2018**, *18*, 3502—3508
- (8) Dahl, J. C.; Osowiecki, W. T.; Cai, Y.; Swabeck, J. K.; Bekenstein, Y.; Asta, M.; Chan, E. M.; Alivisatos, A. P. Probing the Stability and Band Gaps of Cs<sub>2</sub>AgInCl<sub>6</sub> and Cs<sub>2</sub>AgSbCl<sub>6</sub> Lead-Free Double Perovskite Nanocrystals. *Chem. Mater.* **2019**, *31*, 3134–3143. (9) Locardi, F.; Cirignano, M.; Baranov, D.; Dang, Z.; Prato, M.; Drago, F.; Ferretti, M.; Pinchetti, V.; Fanciulli, M.; Brovelli, S.; De
- Drago, F.; Ferretti, M.; Pinchetti, V.; Fanciulli, M.; Brovelli, S.; De Trizio, L.; Manna, L. Colloidal Synthesis of Double Perovskite Cs<sub>2</sub>AgInCl<sub>6</sub> and Mn-Doped Cs<sub>2</sub>AgInCl<sub>6</sub> Nanocrystals. *J. Am. Chem. Soc.* **2018**, *140*, 12989–12995.
- (10) Han, P.; Mao, X.; Yang, S.; Zhang, F.; Yang, B.; Wei, D.; Deng, W.; Han, K. Lead-Free Sodium-Indium Double Perovskite Nanocrystals through Doping Silver Cations for Bright Yellow Emission. *Angew. Chem., Int. Ed.* **2019**, *58*, 17231–17235.
- (11) Wang, L.; Williams, N. E.; Malachosky, E. W.; Otto, J. P.; Hayes, D.; Wood, R. E.; Guyot-Sionnest, P.; Engel, G. S. Scalable Ligand-Mediated Transport Synthesis of Organic-Inorganic Hybrid Perovskite Nanocrystals with Resolved Electronic Structure and Ultrafast Dynamics. ACS Nano 2017, 11, 2689–2696.
- (12) Vybornyi, O.; Yakunin, S.; Kovalenko, M. V. Polar-Solvent-Free Colloidal Synthesis of Highly Luminescent Alkylammonium Lead Halide Perovskite Nanocrystals. *Nanoscale* **2016**, *8*, 6278–6283.
- (13) Minh, D. N.; Kim, J.; Hyon, J.; Sim, J. H.; Sowlih, H. H.; Seo, C.; Nam, J.; Eom, S.; Suk, S.; Lee, S.; Kim, E.; Kang, Y. Room-Temperature Synthesis of Widely Tunable Formamidinium Lead Halide Perovskite Nanocrystals. *Chem. Mater.* **2017**, *29*, 5713–5719.
- (14) Protesescu, L.; Yakunin, S.; Kumar, S.; Bär, J.; Bertolotti, F.; Masciocchi, N.; Guagliardi, A.; Grotevent, M.; Shorubalko, I.; Bodnarchuk, M. I.; Shih, C. J.; Kovalenko, M. V. Dismantling the "Red Wall" of Colloidal Perovskites: Highly Luminescent Formamidinium and Formamidinium-Cesium Lead Iodide Nanocrystals. *ACS Nano* 2017, 11, 3119–3134.
- (15) Weidman, M. C.; Goodman, A. J.; Tisdale, W. A. Colloidal Halide Perovskite Nanoplatelets: An Exciting New Class of Semiconductor Nanomaterials. *Chem. Mater.* **2017**, *29*, 5019–5030.
- (16) Dirin, D. N.; Protesescu, L.; Trummer, D.; Kochetygov, I. V.; Yakunin, S.; Krumeich, F.; Stadie, N. P.; Kovalenko, M. V. Harnessing Defect-Tolerance at the Nanoscale: Highly Luminescent Lead Halide Perovskite Nanocrystals in Mesoporous Silica Matrixes. *Nano Lett.* **2016**, *16*, 5866–5874.
- (17) Huang, H.; Bodnarchuk, M. I.; Kershaw, S. V.; Kovalenko, M. V.; Rogach, A. L. Lead Halide Perovskite Nanocrystals in the Research Spotlight: Stability and Defect Tolerance. *ACS Energy Lett.* **2017**, *2*, 2071–2083.
- (18) Becker, M. A.; Vaxenburg, R.; Nedelcu, G.; Sercel, P. C.; Shabaev, A.; Mehl, M. J.; Michopoulos, J. G.; Lambrakos, S. G.; Bernstein, N.; Lyons, J. L.; Stöferle, T.; Mahrt, R. F.; Kovalenko, M. V.; Norris, D. J.; Rainò, G.; Efros, A. L. Bright Triplet Excitons in Caesium Lead Halide Perovskites. *Nature* **2018**, *553*, 189–193.
- (19) Raino, G.; Becker, M. A.; Bodnarchuk, M. I.; Mahrt, R. F.; Kovalenko, M. V.; Stoferle, T. Superfluorescence from Lead Halide Perovskite Quantum Dot Superlattices. *Nature* **2018**, *563*, *671*–*675*.

- (20) Swarnkar, A.; Marshall, A. R.; Sanehira, E. M.; Chernomordik, B. D.; Moore, D. T.; Christians, J. A.; Chakrabarti, T.; Luther, J. M. Quantum Dot-Induced Phase Stabilization of Alpha-CsPbI<sub>3</sub> Perovskite for High Efficiency Photovoltaics. *Science* **2016**, *354*, 92–95.
- (21) Thomas, C. J.; Zhang, Y.; Guillaussier, A.; Bdeir, K.; Aly, O. F.; Kim, H. G.; Noh, J.; Reimnitz, L. C.; Li, J.; Deepak, F. L.; Smilgies, D.-M.; Milliron, D. J.; Korgel, B. A. Thermal Stability of the Black Perovskite Phase in Cesium Lead Iodide Nanocrystals Under Humid Conditions. *Chem. Mater.* **2019**, *31*, 9750–9758.
- (22) Sanehira, E. M.; Marshall, A. R.; Christians, J. A.; Harvey, S. P.; Ciesielski, P. N.; Wheeler, L. M.; Schulz, P.; Lin, L. Y.; Beard, M. C.; Luther, J. M. Enhanced Mobility CsPbI<sub>3</sub> Quantum Dot Arrays for Record-Efficiency, High-Voltage Photovoltaic Cells. *Sci. Adv.* **2017**, 3, eaao4204.
- (23) Hazarika, A.; Zhao, Q.; Gaulding, E. A.; Christians, J. A.; Dou, B.; Marshall, A. R.; Moot, T.; Berry, J. J.; Johnson, J. C.; Luther, J. M. Perovskite Quantum Dot Photovoltaic Materials beyond the Reach of Thin Films: Full-Range Tuning of A-Site Cation Composition. *ACS Nano* 2018, *12*, 10327–10337.
- (24) Suri, M.; Hazarika, A.; Larson, B. W.; Zhao, Q.; Vallés-Pelarda, M.; Siegler, T. D.; Abney, M. K.; Ferguson, A. J.; Korgel, B. A.; Luther, J. M. Enhanced Open-Circuit Voltage of Wide-Bandgap Perovskite Photovoltaics by Using Alloyed (FA<sub>1-x</sub>Cs<sub>x</sub>)Pb(I<sub>1-x</sub>Br<sub>x</sub>)<sub>3</sub> Quantum Dots. ACS Energy Lett. **2019**, *4*, 1954–1960.
- (25) Akkerman, Q. A.; Gandini, M.; Di Stasio, F.; Rastogi, P.; Palazon, F.; Bertoni, G.; Ball, J. M.; Prato, M.; Petrozza, A.; Manna, L. Strongly Emissive Perovskite Nanocrystal Inks for High-Voltage Solar Cells. *Nat. Energy* **2017**, *2*, 16194.
- (26) El-Ballouli, A. O.; Bakr, O. M.; Mohammed, O. F. Compositional, Processing, and Interfacial Engineering of Nanocrystal- and Quantum-Dot-Based Perovskite Solar Cells. *Chem. Mater.* **2019**, *31*, 6387–6411.
- (27) Hao, M.; Bai, Y.; Zeiske, S.; Ren, L.; Liu, J.; Yuan, Y.; Zarrabi, N.; Cheng, N.; Ghasemi, M.; Chen, P.; Lyu, M.; He, D.; Yun, J. H.; Du, Y.; Wang, Y.; Ding, S.; Armin, A.; Meredith, P.; Liu, G.; Cheng, H. M.; Wang, L. Ligand-Assisted Cation-Exchange Engineering for High-Efficiency Colloidal Cs<sub>1-x</sub>FA<sub>x</sub>PbI<sub>3</sub> Quantum Dot Solar Cells with Reduced Phase Segregation. *Nat. Energy* **2020**, *5*, 79–88.
- (28) Li, G.; Rivarola, F. W. R.; Davis, N. J. L. K.; Bai, S.; Jellicoe, T. C.; de la Peña, F.; Hou, S.; Ducati, C.; Gao, F.; Friend, R. H.; Greenham, N. C.; Tan, Z.-K. Highly Efficient Perovskite Nanocrystal Light-Emitting Diodes Enabled by a Universal Crosslinking Method. *Adv. Mater.* **2016**, *28*, 3528–3534.
- (29) Pan, J.; Quan, L. N.; Zhao, Y.; Peng, W.; Murali, B.; Sarmah, S. P.; Yuan, M.; Sinatra, L.; Alyami, N. M.; Liu, J.; Yassitepe, E.; Yang, Z.; Voznyy, O.; Comin, R.; Hedhili, M. N.; Mohammed, O. F.; Lu, Z. H.; Kim, D. H.; Sargent, E. H.; Bakr, O. M. Highly Efficient Perovskite-Quantum-Dot Light-Emitting Diodes by Surface Engineering. Adv. Mater. 2016, 28, 8718–8725.
- (30) Li, J.; Xu, L.; Wang, T.; Song, J.; Chen, J.; Xue, J.; Dong, Y.; Cai, B.; Shan, Q.; Han, B.; Zeng, H. 50-Fold EQE Improvement up to 6.27% of Solution-Processed All-Inorganic Perovskite CsPbBr<sub>3</sub> QLEDs via Surface Ligand Density Control. *Adv. Mater.* **2017**, 29, 1603885.
- (31) Zhang, X.; Sun, C.; Zhang, Y.; Wu, H.; Ji, C.; Chuai, Y.; Wang, P.; Wen, S.; Zhang, C.; Yu, W. W. Bright Perovskite Nanocrystal Films for Efficient Light-Emitting Devices. *J. Phys. Chem. Lett.* **2016**, 7, 4602–4610.
- (32) Chiba, T.; Hoshi, K.; Pu, Y. J.; Takeda, Y.; Hayashi, Y.; Ohisa, S.; Kawata, S.; Kido, J. High-Efficiency Perovskite Quantum-Dot Light-Emitting Devices by Effective Washing Process and Interfacial Energy Level Alignment. ACS Appl. Mater. Interfaces 2017, 9, 18054—18060.
- (33) Yakunin, S.; Protesescu, L.; Krieg, F.; Bodnarchuk, M. I.; Nedelcu, G.; Humer, M.; De Luca, G.; Fiebig, M.; Heiss, W.; Kovalenko, M. V. Low-Threshold Amplified Spontaneous Emission and Lasing from Colloidal Nanocrystals of Caesium Lead Halide Perovskites. *Nat. Commun.* **2015**, *6*, 8056.

- (34) Eaton, S. W.; Lai, M.; Gibson, N. A.; Wong, A. B.; Dou, L.; Ma, J.; Wang, L.-W.; Leone, S. R.; Yang, P. Lasing in Robust Cesium Lead Halide Perovskite Nanowires. *Proc. Natl. Acad. Sci. U. S. A.* **2016**, *113*, 1993–1998.
- (35) Zhang, J.; Wang, Q.; Zhang, X.; Jiang, J.; Gao, Z.; Jin, Z.; Liu, S. High-Performance Transparent Ultraviolet Photodetectors Based on Inorganic Perovskite CsPbCl<sub>3</sub> Nanocrystals. *RSC Adv.* **2017**, 7, 36722–36727.
- (36) Surendran, A.; Yu, X.; Begum, R.; Tao, Y.; Wang, Q. J.; Leong, W. L. All Inorganic Mixed Halide Perovskite Nanocrystal—Graphene Hybrid Photodetector: From Ultrahigh Gain to Photostability. *ACS Appl. Mater. Interfaces* **2019**, *11*, 27064–27072.
- (37) MØLLER, C. K. Crystal Structure and Photoconductivity of Caesium Plumbohalides. *Nature* **1958**, *182*, 1436.
- (38) Steele, J. A.; Jin, H.; Dovgaliuk, I.; Berger, R. F.; Braeckevelt, T.; Yuan, H.; Martin, C.; Solano, E.; Lejaeghere, K.; Rogge, S. M. J.; Notebaert, C.; Vandezande, W.; Janssen, K. P.F.; Goderis, B.; Debroye, E.; Wang, Y. K.; Dong, Y.; Ma, D.; Saidaminov, M.; Tan, H.; Lu, Z.; Dyadkin, V.; Chernyshov, D.; Van Speybroeck, V.; Sargent, E. H.; Hofkens, J.; Roeffaers, M. B. J. Thermal Unequilibrium of Strained Black CsPbI<sub>3</sub> Thin Films. *Science* **2019**, *365*, *679*–*684*.
- (39) Straus, D. B.; Guo, S.; Cava, R. J. Kinetically Stable Single Crystals of Perovskite-Phase CsPbI<sub>3</sub>. *J. Am. Chem. Soc.* **2019**, *141*, 11435–11439.
- (40) Imran, M.; Ijaz, P.; Baranov, D.; Goldoni, L.; Petralanda, U.; Akkerman, Q.; Abdelhady, A. L.; Prato, M.; Bianchini, P.; Infante, I.; Manna, L. Shape-Pure, Nearly Monodispersed CsPbBr<sub>3</sub> Nanocubes Prepared Using Secondary Aliphatic Amines. *Nano Lett.* **2018**, *18*, 7822–7831.
- (41) Dutta, A.; Pradhan, N. Phase-Stable Red-Emitting CsPbI<sub>3</sub> Nanocrystals: Successes and Challenges. ACS Energy Lett. **2019**, 4, 709–719.
- (42) Liu, F.; Zhang, Y.; Ding, C.; Kobayashi, S.; Izuishi, T.; Nakazawa, N.; Toyoda, T.; Ohta, T.; Hayase, S.; Minemoto, T.; Yoshino, K.; Dai, S.; Shen, Q. Highly Luminescent Phase-Stable CsPbI<sub>3</sub> Perovskite Quantum Dots Achieving Near 100% Absolute Photoluminescence Quantum Yield. ACS Nano 2017, 11, 10373—10383.
- (43) Cai, Y.; Wang, H.; Li, Y.; Wang, L.; Lv, Y.; Yang, X.; Xie, R. J. Trimethylsilyl Iodine-Mediated Synthesis of Highly Bright Red-Emitting CsPbI<sub>3</sub> Perovskite Quantum Dots with Significantly Improved Stability. *Chem. Mater.* **2019**, *31*, 881–889.
- (44) Imran, M.; Caligiuri, V.; Wang, M.; Goldoni, L.; Prato, M.; Krahne, R.; De Trizio, L.; Manna, L. Benzoyl Halides as Alternative Precursors for the Colloidal Synthesis of Lead-Based Halide Perovskite Nanocrystals. *J. Am. Chem. Soc.* **2018**, *140*, 2656–2664.
- (45) Akkerman, Q. A.; Martínez-Sarti, L.; Goldoni, L.; Imran, M.; Baranov, D.; Bolink, H. J.; Palazon, F.; Manna, L. Molecular Iodine for a General Synthesis of Binary and Ternary Inorganic and Hybrid Organic-Inorganic Iodide Nanocrystals. *Chem. Mater.* **2018**, *30*, 6915–6921.
- (46) Liu, F.; Ding, C.; Zhang, Y.; Kamisaka, T.; Zhao, Q.; Luther, J. M.; Toyoda, T.; Hayase, S.; Minemoto, T.; Yoshino, K.; Zhang, B.; Dai, S.; Jiang, J.; Tao, S.; Shen, Q. GeI<sub>2</sub> Additive for High Optoelectronic Quality CsPbI<sub>3</sub> Quantum Dots and Their Application in Photovoltaic Devices. *Chem. Mater.* **2019**, *31*, 798–807.
- (47) Hosomi, A.; Sakurai, H. Protection of Alcohols and Acids With Allylsilanes Catalyzed By Iodine or Iodotrimethylsilane in Chlorinated Hydrocarbon. *Chem. Lett.* **1981**, *10*, 85–88.
- (48) Fessenden, R.; Fessenden, J. S. The Chemistry of Silicon-Nitrogen Compounds. *Chem. Rev.* **1961**, *61*, 361–388.
- (49) Travis, W.; Glover, E. N. K.; Bronstein, H.; Scanlon, D. O.; Palgrave, R. G. On the Application of the Tolerance Factor to Inorganic and Hybrid Halide Perovskites: A Revised System. *Chem. Sci.* **2016**, *7*, 4548–4556.
- (50) Cottingham, P.; Brutchey, R. L. Depressed Phase Transitions and Thermally Persistent Local Distortions in CsPbBr<sub>3</sub> Quantum Dots. *Chem. Mater.* **2018**, *30*, 6711–6716.

- (51) Seth, S.; Ahmed, T.; De, A.; Samanta, A. Tackling the Defects, Stability, and Photoluminescence of CsPbX<sub>3</sub> Perovskite Nanocrystals. *ACS Energy Lett.* **2019**, *4*, 1610–1618.
- (52) De Roo, J.; Ibáñez, M.; Geiregat, P.; Nedelcu, G.; Walravens, W.; Maes, J.; Martins, J. C.; Van Driessche, I.; Kovalenko, M. V.; Hens, Z. Highly Dynamic Ligand Binding and Light Absorption Coefficient of Cesium Lead Bromide Perovskite Nanocrystals. *ACS Nano* **2016**, *10*, 2071–2081.
- (53) Almeida, G.; Goldoni, L.; Akkerman, Q.; Dang, Z.; Khan, A. H.; Marras, S.; Moreels, I.; Manna, L. Role of Acid-Base Equilibria in the Size, Shape, and Phase Control of Cesium Lead Bromide Nanocrystals. *ACS Nano* **2018**, *12*, 1704–1711.
- (54) Parobek, D.; Dong, Y.; Qiao, T.; Son, D. H. Direct Hot-Injection Synthesis of Mn-Doped CsPbBr<sub>3</sub> Nanocrystals. *Chem. Mater.* **2018**, *30*, 2939–2944.
- (55) Cao, W.; Liu, P.; Chen, W.; Wang, W.; Xu, B.; Wu, D.; Hao, J.; Cao, W.; Fang, F.; Li, Y.; Zeng, Y.; Pan, R.; Chen, S.; Sun, X. W.; Wang, K. Halide-Rich Synthesized Cesium Lead Bromide Perovskite Nanocrystals for Light-Emitting Diodes with Improved Performance. *Chem. Mater.* 2017, 29, 5168–5173.
- (56) Wen, J. R.; Roman, B. J.; Rodriguez Ortiz, F. A.; Mireles Villegas, N.; Porcellino, N.; Sheldon, M. Chemical Availability of Bromide Dictates CsPbBr<sub>3</sub> Nanocrystal Growth. *Chem. Mater.* **2019**, *31*, 8551–8557.
- (57) Juarez-Perez, E. J.; Hawash, Z.; Raga, S. R.; Ono, L. K.; Qi, Y. Thermal Degradation of CH<sub>3</sub>NH<sub>3</sub>PbI<sub>3</sub> Perovskite into NH<sub>3</sub> and CH<sub>3</sub>I Gases Observed by Coupled Thermogravimetry—Mass Spectrometry Analysis. *Energy Environ. Sci.* **2016**, *9*, 3406–3410.
- (58) Ma, L.; Guo, D.; Li, M.; Wang, C.; Zhou, Z.; Zhao, X.; Zhang, F.; Ao, Z.; Nie, Z. Temperature-Dependent Thermal Decomposition Pathway of Organic-Inorganic Halide Perovskite Materials. *Chem. Mater.* **2019**, *31*, 8515–8522.
- (59) Zhang, Y.; Thomas, C. J.; Guillaussier, A.; Smilgies, D.-M.; Korgel, B. A. Thermal Phase Transitions in Superlattice Assemblies of Cuboidal CH<sub>3</sub>NH<sub>3</sub>PbI<sub>3</sub> Nanocrystals Followed by Grazing Incidence X-Ray Scattering. *J. Phys. Chem. C* **2019**, *123*, 17555–17565.
- (60) Zhang, Y.; Shah, T.; Deepak, F. L.; Korgel, B. A. Surface Science and Colloidal Stability of Double Perovskite Cs<sub>2</sub>AgBiBr<sub>6</sub> Nanocrystals and Their Superlattices. *Chem. Mater.* **2019**, *31*, 7962–7060
- (61) Shi, D.; Adinolfi, V.; Comin, R.; Yuan, M.; Alarousu, E.; Buin, A.; Chen, Y.; Hoogland, S.; Rothenberger, A.; Katsiev, K.; Losovyj, Y.; Zhang, X.; Dowben, P. A.; Mohammed, O. F.; Sargent, E. H.; Bakr, O. M. Low Trap-State Density and Long Carrier Diffusion in Organolead Trihalide Perovskite Single Crystals. *Science* 2015, 347, 519–522.
- (62) Mcclure, E. T.; Ball, M. R.; Windl, W.; Woodward, P. M. Cs<sub>2</sub>AgBiX<sub>6</sub> (X = Br,Cl): New Visible Light Absorbing, Lead-Free Halide Perovskite Semiconductors. *Chem. Mater.* **2016**, 28, 1348–1354
- (63) Slavney, A. H.; Hu, T.; Lindenberg, A. M.; Karunadasa, H. I. A Bismuth-Halide Double Perovskite with Long Carrier Recombination Lifetime for Photovoltaic Applications. *J. Am. Chem. Soc.* **2016**, *138*, 2138–2141.
- (64) Lu, C.; Wright, M. W.; Ma, X.; Li, H.; Itanze, D. S.; Carter, J. A.; Hewitt, C. A.; Donati, G. L.; Carroll, D. L.; Lundin, P. M.; Geyer, S. M. Cesium Oleate Precursor Preparation for Lead Halide Perovskite Nanocrystal Synthesis: The Influence of Excess Oleic Acid on Achieving Solubility, Conversion, and Reproducibility. *Chem. Mater.* **2019**, *31*, 62–67.
- (65) Almeida, G.; Ashton, O. J.; Goldoni, L.; Maggioni, D.; Petralanda, U.; Mishra, N.; Akkerman, Q. A.; Infante, I.; Snaith, H. J.; Manna, L. The Phosphine Oxide Route toward Lead Halide Perovskite Nanocrystals. *J. Am. Chem. Soc.* 2018, 140, 14878–14886. (66) Ravi, V. K.; Santra, P. K.; Joshi, N.; Chugh, J.; Singh, S. K.; Rensmo, H.; Ghosh, P.; Nag, A. Origin of the Substitution Mechanism for the Binding of Organic Ligands on the Surface of CsPbBr<sub>3</sub> Perovskite Nanocubes. *J. Phys. Chem. Lett.* 2017, 8, 4988–4994.

- (67) Wang, C.; Chesman, S. R.; Jasieniak, J. J. Stabilizing the Cubic Perovskite Phase of CsPbI<sub>3</sub> Nanocrystals by Using an Alkyl Phosphinic Acid. *Chem. Commun.* **2017**, *53*, 232–235.
- (68) Grisorio, R.; Di Clemente, M. E.; Fanizza, E.; Allegretta, I.; Altamura, D.; Striccoli, M.; Terzano, R.; Giannini, C.; Irimia-Vladu, M.; Suranna, G. P. Exploring the Surface Chemistry of Cesium Lead Halide Perovskite Nanocrystals. *Nanoscale* **2019**, *11*, 986–999.
- (69) Pan, A.; He, B.; Fan, X.; Liu, Z.; Urban, J. J.; Alivisatos, A. P.; He, L.; Liu, Y. Insight into the Ligand-Mediated Synthesis of Colloidal CsPbBr<sub>3</sub> Perovskite Nanocrystals: The Role of Organic Acid, Base, and Cesium Precursors. *ACS Nano* **2016**, *10*, 7943–7954.
- (70) Aharon, S.; Wierzbowska, M.; Etgar, L. The Effect of the Alkylammonium Ligand's Length on Organic-Inorganic Perovskite Nanoparticles. *ACS Energy Lett.* **2018**, *3*, 1387–1393.
- (71) Liang, Z.; Zhao, S.; Xu, Z.; Qiao, B.; Song, P.; Gao, D.; Xu, X. Shape-Controlled Synthesis of All-Inorganic CsPbBr<sub>3</sub> Perovskite Nanocrystals with Bright Blue Emission. *ACS Appl. Mater. Interfaces* **2016**, *8*, 28824–28830.
- (72) Saidaminov, M. I.; Almutlaq, J.; Sarmah, S.; Dursun, I.; Zhumekenov, A. A.; Begum, R.; Pan, J.; Cho, N.; Mohammed, O. F.; Bakr, O. M. Pure Cs<sub>4</sub>PbBr<sub>6</sub>: Highly Luminescent Zero-Dimensional Perovskite Solids. *ACS Energy Lett.* **2016**, *1*, 840–845.
- (73) Zhang, Y.; Saidaminov, M. I.; Dursun, I.; Yang, H.; Murali, B.; Alarousu, E.; Yengel, E.; Alshankiti, B. A.; Bakr, O. M.; Mohammed, O. F. Zero-Dimensional Cs<sub>4</sub>PbBr<sub>6</sub> Perovskite Nanocrystals. *J. Phys. Chem. Lett.* **2017**, *8*, 961–965.
- (74) Qin, Z.; Dai, S.; Hadjiev, V. G.; Wang, C.; Xie, L.; Ni, Y.; Wu, C.; Yang, G.; Chen, S.; Deng, L.; Yu, Q.; Feng, G.; Wang, Z. M.; Bao, J. Revealing the Origin of Luminescence Center in 0D  $Cs_4PbBr_6$  Perovskite. *Chem. Mater.* **2019**, *31*, 9098–9104.
- (75) Palazon, F.; Almeida, G.; Akkerman, Q. A.; De Trizio, L.; Dang, Z.; Prato, M.; Manna, L. Changing the Dimensionality of Cesium Lead Bromide Nanocrystals by Reversible Postsynthesis Transformations with Amines. *Chem. Mater.* **2017**, *29*, 4167–4171.
- (76) Udayabhaskararao, T.; Houben, L.; Cohen, H.; Menahem, M.; Pinkas, I.; Avram, L.; Wolf, T.; Teitelboim, A.; Leskes, M.; Yaffe, O.; Oron, D.; Kazes, M. A Mechanistic Study of Phase Transformation in Perovskite Nanocrystals Driven by Ligand Passivation. *Chem. Mater.* **2018**, *30*, 84–93.
- (77) Akkerman, Q. A.; Park, S.; Radicchi, E.; Nunzi, F.; Mosconi, E.; De Angelis, F.; Brescia, R.; Rastogi, P.; Prato, M.; Manna, L. Nearly Monodisperse Insulator Cs<sub>4</sub>PbX<sub>6</sub> (X = Cl, Br, I) Nanocrystals, Their Mixed Halide Compositions, and Their Transformation into CsPbX<sub>3</sub> Nanocrystals. *Nano Lett.* **2017**, *17*, 1924–1930.
- (78) Koh, W.; Park, S.; Ham, Y. Phosphonic Acid Stabilized Colloidal CsPbX<sub>3</sub> (X = Br, I) Perovskite Nanocrystals and Their Surface Chemistry. *ChemistrySelect* **2016**, *1*, 3479–3482.
- (79) Krieg, F.; Ochsenbein, S. T.; Yakunin, S.; Ten Brinck, S.; Aellen, P.; Süess, A.; Clerc, B.; Guggisberg, D.; Nazarenko, O.; Shynkarenko, Y.; Kumar, S.; Shih, C. J.; Infante, I.; Kovalenko, M. V. Colloidal CsPbX<sub>3</sub> (X = Cl, Br, I) Nanocrystals 2.0: Zwitterionic Capping Ligands for Improved Durability and Stability. *ACS Energy Lett.* 2018, 3, 641–646.
- (80) Dutta, A.; Behera, R. K.; Dutta, S. K.; Das Adhikari, S.; Pradhan, N. Annealing  $CsPbX_3$  (X = Cl and Br) Perovskite Nanocrystals at High Reaction Temperatures: Phase Change and Its Prevention. *J. Phys. Chem. Lett.* **2018**, *9*, 6599–6604.
- (81) Dutta, A.; Dutta, S. K.; Das Adhikari, S.; Pradhan, N. Phase-Stable CsPbI<sub>3</sub> Nanocrystals: The Reaction Temperature Matters. *Angew. Chem., Int. Ed.* **2018**, *57*, 9083–9087.
- (82) Liu, Z.; Bekenstein, Y.; Ye, X.; Nguyen, S. C.; Swabeck, J.; Zhang, D.; Lee, S. T.; Yang, P.; Ma, W.; Alivisatos, A. P. Ligand Mediated Transformation of Cesium Lead Bromide Perovskite Nanocrystals to Lead Depleted Cs<sub>4</sub>PbBr<sub>6</sub> Nanocrystals. *J. Am. Chem. Soc.* **2017**, *139*, 5309–5312.
- (83) Pradhan, N. Tips and Twists in Making High Photoluminescence Quantum Yield Perovskite Nanocrystals. *ACS Energy Lett.* **2019**, *4*, 1634–1638.

- (84) Zhang, D.; Eaton, S. W.; Yu, Y.; Dou, L.; Yang, P. Solution-Phase Synthesis of Cesium Lead Halide Perovskite Nanowires. *J. Am. Chem. Soc.* **2015**, *137*, 9230–9233.
- (85) Bertolotti, F.; Protesescu, L.; Kovalenko, M. V.; Yakunin, S.; Cervellino, A.; Billinge, S. J. L.; Terban, M. W.; Pedersen, J. S.; Masciocchi, N.; Guagliardi, A. Coherent Nanotwins and Dynamic Disorder in Cesium Lead Halide Perovskite Nanocrystals. *ACS Nano* **2017**, *11*, 3819–3831.
- (86) Sutton, R. J.; Filip, M. R.; Haghighirad, A. A.; Sakai, N.; Wenger, B.; Giustino, F.; Snaith, H. J. Cubic or Orthorhombic? Revealing the Crystal Structure of Metastable Black-Phase CsPbI<sub>3</sub> by Theory and Experiment. *ACS Energy Lett.* **2018**, *3*, 1787–1794.
- (87) Bodnarchuk, M. I.; Boehme, S. C.; Ten Brinck, S.; Bernasconi, C.; Shynkarenko, Y.; Krieg, F.; Widmer, R.; Aeschlimann, B.; Günther, D.; Kovalenko, M. V.; Infante, I. Rationalizing and Controlling the Surface Structure and Electronic Passivation of Cesium Lead Halide Nanocrystals. ACS Energy Lett. 2019, 4, 63–74.
- (88) Sun, J. K.; Huang, S.; Liu, X. Z.; Xu, Q.; Zhang, Q. H.; Jiang, W. J.; Xue, D. J.; Xu, J. C.; Ma, J. Y.; Ding, J.; Ge, Q. Q.; Gu, L.; Fang, X. H.; Zhong, H. Z.; Hu, J. S.; Wan, L. J. Polar Solvent Induced Lattice Distortion of Cubic CsPbI<sub>3</sub> Nanocubes and Hierarchical Self-Assembly into Orthorhombic Single-Crystalline Nanowires. *J. Am. Chem. Soc.* 2018, 140, 11705–11715.
- (89) Jiang, Y.; Qin, C.; Cui, M.; He, T.; Liu, K.; Huang, Y.; Luo, M.; Zhang, L.; Xu, H.; Li, S.; Wei, J.; Liu, Z.; Wang, H.; Kim, G. H.; Yuan, M.; Chen, J. Spectra Stable Blue Perovskite Light-Emitting Diodes. *Nat. Commun.* **2019**, *10*, 1868.
- (90) Kim, Y.; Yassitepe, E.; Voznyy, O.; Comin, R.; Walters, G.; Gong, X.; Kanjanaboos, P.; Nogueira, A. F.; Sargent, E. H. Efficient Luminescence from Perovskite Quantum Dot Solids. *ACS Appl. Mater. Interfaces* **2015**, *7*, 25007–25013.
- (91) Reichardt, C. Solvents and Solvent Effects in Organic Chemistry, 3rd ed.; Wiley-VCH: 2003.
- (92) Nenon, D. P.; Pressler, K.; Kang, J.; Koscher, B. A.; Olshansky, J. H.; Osowiecki, W. T.; Koc, M. A.; Wang, L. W.; Alivisatos, A. P. Design Principles for Trap-Free CsPbX<sub>3</sub> Nanocrystals: Enumerating and Eliminating Surface Halide Vacancies with Softer Lewis Bases. J. Am. Chem. Soc. 2018, 140, 17760–17772.
- (93) Huang, S.; Li, Z.; Wang, B.; Zhu, N.; Zhang, C.; Kong, L.; Zhang, Q.; Shan, A.; Li, L. Morphology Evolution and Degradation of CsPbBr<sub>3</sub> Nanocrystals under Blue Light-Emitting Diode Illumination. *ACS Appl. Mater. Interfaces* **2017**, *9*, 7249–7258.
- (94) Liu, J.; Song, K.; Shin, Y.; Liu, X.; Chen, J.; Yao, K. X.; Pan, J.; Yang, C.; Yin, J.; Xu, L. J.; Yang, H.; El-Zohry, A. M.; Xin, B.; Mitra, S.; Hedhili, M. N.; Roqan, I. S.; Mohammed, O. F.; Han, Y.; Bakr, O. M. Light-Induced Self-Assembly of Cubic CsPbBr<sub>3</sub> Perovskite Nanocrystals into Nanowires. *Chem. Mater.* **2019**, *31*, 6642–6649.
- (95) Almeida, G.; Infante, I.; Manna, L. Resurfacing Halide Pperovskite Nanocrystals. *Science* **2019**, *364*, 833–834.
- (96) Imran, M.; Ijaz, P.; Goldoni, L.; Maggioni, D.; Petralanda, U.; Prato, M.; Almeida, G.; Infante, I.; Manna, L. Simultaneous Cationic and Anionic Ligand Exchange for Colloidally Stable CsPbBr<sub>3</sub> Nanocrystals. ACS Energy Lett. **2019**, *4*, 819–824.
- (97) Tan, Y.; Zou, Y.; Wu, L.; Huang, Q.; Yang, D.; Chen, M.; Ban, M.; Wu, C.; Wu, T.; Bai, S.; Song, T.; Zhang, Q.; Sun, B. Highly Luminescent and Stable Perovskite Nanocrystals with Octylphosphonic Acid as a Ligand for Efficient Light-Emitting Diodes. ACS Appl. Mater. Interfaces 2018, 10, 3784–3792.
- (98) Wang, H.; Sui, N.; Bai, X.; Zhang, Y.; Rice, Q.; Seo, F. J.; Zhang, Q.; Colvin, V. L.; Yu, W. W. Emission Recovery and Stability Enhancement of Inorganic Perovskite Quantum Dots. *J. Phys. Chem. Lett.* **2018**, *9*, 4166–4173.
- (99) Alpert, M. R.; Niezgoda, J. S.; Chen, A. Z.; Foley, B. J.; Cuthriell, S.; Yoon, L. U.; Choi, J. J. Colloidal Nanocrystals as a Platform for Rapid Screening of Charge Trap Passivating Molecules for Metal Halide Perovskite Thin Films. *Chem. Mater.* **2018**, *30*, 4515–4526.
- (100) Pan, J.; Shang, Y.; Yin, J.; De Bastiani, M.; Peng, W.; Dursun, I.; Sinatra, L.; El-Zohry, A. M.; Hedhili, M. N.; Emwas, A. H.;

- Mohammed, O. F.; Ning, Z.; Bakr, O. M. Bidentate Ligand-Passivated CsPbI<sub>3</sub> Perovskite Nanocrystals for Stable Near-Unity Photoluminescence Quantum Yield and Efficient Red Light-Emitting Diodes. *J. Am. Chem. Soc.* **2018**, *140*, 562–565.
- (101) Koscher, B. A.; Swabeck, J. K.; Bronstein, N. D.; Alivisatos, A. P. Essentially Trap-Free CsPbBr<sub>3</sub> Colloidal Nanocrystals by Postsynthetic Thiocyanate Surface Treatment. *J. Am. Chem. Soc.* **2017**, *139*, 6566–6569.
- (102) Ahmed, T.; Seth, S.; Samanta, A. Boosting the Photoluminescence of  $CsPbX_3$  (X = Cl, Br, I) Perovskite Nanocrystals Covering a Wide Wavelength Range by Postsynthetic Treatment with Tetrafluoroborate Salts. *Chem. Mater.* **2018**, *30*, 3633–3637.
- (103) Leguy, M. A.; Hu, Y.; Campoy-quiles, M.; Alonso, M. I.; Weber, O. J.; Azarhoosh, P.; van Schilfgaarde, M.; Weller, M. T.; Bein, T.; Nelson, J.; Docampo, P.; Barnes, P. R. F. Reversible Hydration of CH<sub>3</sub>NH<sub>3</sub>PbI<sub>3</sub> in Films, Single Crystals, and Solar Cells. *Chem. Mater.* **2015**, 27, 3397–3407.
- (104) Li, Y.; Zhou, W.; Li, Y.; Huang, W.; Zhang, Z.; Chen, G.; Wang, H.; Wu, G.-H.; Rolston, N.; Vila, R.; Chiu, W.; Cui, Y. Unravelling Degradation Mechanisms and Atomic Structure of Organic-Inorganic Halide Perovskites by Cryo-EM. *Joule* 2019, 3, 2854–2866.
- (105) Yu, Y.; Zhang, D.; Kisielowski, C.; Dou, L.; Kornienko, N.; Bekenstein, Y.; Wong, A. B.; Alivisatos, A. P.; Yang, P. Atomic Resolution Imaging of Halide Perovskites. *Nano Lett.* **2016**, *16*, 7530–7535.
- (106) Dang, Z.; Shamsi, J.; Palazon, F.; Imran, M.; Akkerman, Q. A.; Park, S.; Bertoni, G.; Prato, M.; Brescia, R.; Manna, L. In Situ Transmission Electron Microscopy Study of Electron Beam-Induced Transformations in Colloidal Cesium Lead Halide Perovskite Nanocrystals. *ACS Nano* **2017**, *11*, 2124–2132.
- (107) Gomez, L.; Lin, J.; De Weerd, C.; Poirier, L.; Boehme, S. C.; Von Hauff, E.; Fujiwara, Y.; Suenaga, K.; Gregorkiewicz, T. Extraordinary Interfacial Stitching between Single All-Inorganic Perovskite Nanocrystals. ACS Appl. Mater. Interfaces 2018, 10, 5984–5991.
- (108) Rothmann, M. U.; Li, W.; Zhu, Y.; Liu, A.; Ku, Z.; Bach, U.; Etheridge, J.; Cheng, Y. B. Structural and Chemical Changes to CH<sub>3</sub>NH<sub>3</sub>PbI<sub>3</sub> Induced by Electron and Gallium Ion Beams. *Adv. Mater.* **2018**, *30*, 1800629.
- (109) Chen, S.; Zhang, X.; Zhao, J.; Zhang, Y.; Kong, G.; Li, Q.; Li, N.; Yu, Y.; Xu, N.; Zhang, J.; Liu, K.; Zhao, Q.; Cao, J.; Feng, J.; Li, X.; Qi, J.; Yu, D.; Li, J.; Gao, P. Atomic Scale Insights into Structure Instability and Decomposition Pathway of Methylammonium Lead Iodide Perovskite. *Nat. Commun.* **2018**, *9*, 4807.